Responses to Referees' Comments on "S2P3-R (v1.0): a framework for efficient regional modelling of physical and biological structures and processes in shelf seas" by R. Marsh et al. (gmd-2014-256)

Overview of Responses

We thank the referees for extensive and informative comments. Below, we list these verbatim (italic text), responding to each comment in turn. In the revised manuscript, the revised text is highlighted in red.

Response to Referee #1

General Comments:

One main comment, which I think is fundamental. I like the model system presented but the model system is based on the S2P3 modelling system. This already exists and is published elsewhere. The title and text outline "the provision of a practical tool for linking theory and observations", whereas reading this I would argue that you are providing an evaluation based on a number of case-study examples. I would agree that this is useful and important but it is not clear what is novel about the S2P3-R framework apart from some source code changes and implementation in differing domains. If there are no other changes, I would present the study differently or I would highlight the differences between the S2P3-R and S2P3 more explicitly. Generally though a well-written paper I found informative. I only have issues with the framework context, which may not really be that much of a concern for the GMD format compared to other journals.

Response: In the revised manuscript, we emphasize that S2P3 as currently available has not been extensively used/tested across transects or in regions where the dominance of 1D (vertical) processes mean that the model can be appropriately used for efficiently investigating 3D time-evolving structures (lines 69-72). Since submission of the manuscript, S2P3-R has been further used to investigate seasonal development of stratification and the sub-surface chlorophyll maximum across a wider region (3-9°W, 49-51°N), at 1-km resolution (see Fig. 11 in the revised manuscript, and accompanying text, lines 647-654). Such studies are now easily facilitated with the S2P3-R framework.

Specific Comments (each followed by Response):

Line 13: what is meant by realistic geographical domains as I find this ambiguous?

By "realistic geographical domains", we contrast with previous extensive use of S2P3 in semi-idealized settings. We have revised this opening sentence of the abstract (lines 13-15) as "An established 1-dimensional model of Shelf Sea Physics and Primary Production (S2P3) is adapted for flexible use in selected regional settings and over selected periods of time."

Line 14: does the –R actually mean anything? Reanalysis? Again the significance of S2P3-R over the S2P3 model.

"The "-R" indicates the regional version of S2P3. For clarification, we have revised the second sentence in the abstract (lines 15-16) as "This Regional adaptation of S2P3, the S2P3-R framework (v1.0), can be efficiently used …"

Line 36: The S2P3 does provide an efficient tool for addressing numerous scientific questions but I would argue choice of model depends on the question. For example, if your question concerns lateral advective processes, you require a different type of model. Practicality

would not be an issue, more what modelling tool is required.

As emphasized in our response to the referee's main concern, the model is appropriately used where 1D (vertical) processes dominate 2D (horizontal) processes across much of the shelf seas where we have the observations necessary for a co-evaluation of these processes (lines 625-628). In recognition of this issue, we have developed the text accordingly in various places (lines 471-474, 689-692, 693-699) [See also our response to Referee 2].

Line 40: Something simple in the text to clarify the 1D nature of S2P3, which will make the transition to 3D later in the intro clearer.

We have added to the Introduction (lines 43-45) a brief explanation of the 1D processes represented in S2P3, "S2P3 explicitly represents vertical heat fluxes, vertical mixing of momentum, and vertical mixing of heat and tracers (nitrate and chlorophyll concentrations)."

Line 44: exaggerates the problem I have with the text. If this information is on the website, why do I need to read this paper? What is the novelty of the framework stated in the title?

We have re-phrased our reference to the website (lines 59-61). The framework presented here (modified source code and ancillary files) is new and is not accessible via the current hosting website.

Line 51: I don't agree with the way this is written. The physics you are describing can be implemented, and is implemented elsewhere. Granted there is a practicality to implementing fine-scale physics operationally but it is not that this model can do a better job, which is how a general reader could understand this sentence. If you disagree with differing responses in the simulations, I would expect to see a figure demonstrating this.

We have re-phrased the corresponding text to emphasize that our simpler approach produces results comparable with those obtained from more complex, hence expensive, models (lines 637-646). We provide evidence for this by comparison with a recent simulation with the UK Met Office forecast system (O'Dea et al., 2012), which actually has the same coarse resolution as our northwest European shelf domain. We specifically point out that Fig. 3a in our manuscript - summer surface-bottom temperature differences across the northwest European shelf, with fronts identified - bears close resemblence to the model results in Fig. 10 in O'Dea et al. (2012).

Reference:
O'Dea, E.J., Arnold, A.K., Edwards, K.P., Furner, R., Hyder, P., Martin, M.J., Siddom, J.R., Storkey, D., While, J., Holt, J.T., and H. Liu (2012). An operational ocean forecast system incorporating NEMO and SST data assimilation for the tidally driven European North-West shelf. *Journal of Operational Oceanography*, 5 (1). 3-17.

Line 59: repeated link to the Jon Sharples website, the first reference doesn't seem necessary if you didn't have the earlier quote.

We removed the earlier quote.

Lines 64/72: I understand the importance of S2P3 as an educational tool, but two references to this in two consecutive paragraphs could be streamlined.

We removed the second reference to educational contexts.

Line 91: "very little changed" can be better phrased

We do not need to mention any specific changes, so this text is removed.

Line 178: "aborpton"

Corrected.

Line 184: I don't think it's correct to use colons in a list manner like this?

We have corrected out use of colons throughout Sect. 2.1.

Line 233: grammar - comma placements

We are unclear on what to correct here – no change.

Line 247: the extension of S2P3 is something for the discussion

We have moved this to the discussion, now evidenced in new Fig. 11 and accompanying text (lines 647-654).

Line 254: SCM not defined

We clarify the SCM being defined here as: "sub-surface chl-a maximum (SCM)" (lines 251-252)

Line 259: CTD not defined

We define "Conductivity Temperature Depth (CTD)". (line 257)

Line 271: "temperature for each domain"

We clarify here, and in Table 1, the "initial temperature field". (line 270)

Line 273: and the more coastal Scotland domain was for climate and ecosystem changes as well?

We have removed the "Around Scotland" example, as this largely replicates the "northwest European shelf" example (see below). We do, however, retain the regional example of initial temperature sensitivity in the northeast sub-region of our northwest European shelf domain (hence Fig. S3), slightly revising the text in Sect. 2.3 accordingly (lines 300-309).

Line 278: "emphasised" mixed anglo-amercian spelling

We have corrected the spelling as "emphasized".

Line 280: there seems no context to go with the more coastal North Sea simulations compared to the other three simulations

We removed the "Around Scotland" simulations (text and figures, except Fig. S3), as this largely replicates the "northwest European shelf" simulation.

Line 308: rework sentence

This long sentence is split and revised as follows: "For the China Seas, we specify a higher initial temperature of 15.1°C and simulate two consecutive years, accounting for weak wintertime stratification in this region. We analyse only the second year, for which more

realistic initial conditions are thus established across the wider domain (on 1 January of the second year)." (lines 309-313)

Line 376: "... in particular the Irish Sea and parts of the English Channel are consistent ..."

The referee has misunderstood the meaning of this sentence. We now split the sentence as follows: "Net heat fluxes are also notably positive in some regions that are well mixed all year round, in particular the Irish Sea and parts of the English Channel. This is consistent with enhanced heat storage due to mixing throughout the water column of heat gained in summer (Simpson and Bowers 1984)." (lines 377-381)

Line 381: temperatures?

Corrected as "temperature" (line 375).

Line 383: "locations, artefacts can be introduced to the forcing. This depends on..."

Corrected (line 386).

Line 395: where nutrients are

Corrected (line 397).

Line 405: split the sentence up

We now split the sentence as follows: "Moving towards stratified regions, annual-mean carbon production rates generally decline, although remain above 55 g C m^{-2} year^{-1} at most locations due to the combined result of the major spring and minor autumn blooms (see below). This decline is complemented by elevated productivity throughout summer at the thermocline, associated with the development and persistence of the sub-surface chl-a maximum (SCM)." (lines 407-412)

Line 443: limitation

Corrected (line 445).

Line 476: There is also scope..

We have now removed the short sub-section where this text appears.

Line 515: Here, seasonal cycles ...

We now start a new sentence here (line 507).

Line 523: "while simulated each year separately"?

For clarity, we revised this text as follows: "Starting on 1 January 2002, we simulate one year at a time, specifying a mixed water column temperature on, e.g., 1 January 2003 with the corresponding temperature on 31 December 2002, etc. This ensures continuity in temperatures between years, respecting a small degree of interannual variability in wintertime temperature at L4 and E1." (lines 515-519)

Response to Referee #2

In this manuscript the authors apply a 1D physical-biological framework in a regional implementation in select years and select shelf regions.

General comments:

Although the manuscript is well written, I feel that the content is more suitable for a technical report appearing on a modeling website, than a peer-reviewed publication in GMD. Manuscripts within GMD are expected to "represent a substantial contribution to modeling science", which I do not feel is the case for this manuscript. Furthermore, although the modeling framework discussed here could potentially be useful in an undergraduate ocean modeling curriculum, it is not clear to me that the S2P3-R model has "the potential to perform calculations leading to significant scientific results" as would be required for publication in GMD.

Response: The utility of S2P3-R in undergraduate (and postgraduate) level projects does not preclude its ongoing and future use in research contexts. In regions where shelf sea physics (and biology) is dominated by vertical processes, the framework facilitates experiments to investigate the sensitivity of measurable quantities (e.g., chlorophyll concentration) to a wide range of physical and biological processes that can be adjusted with corresponding model parameters. Where high quality observations are available (e.g., E1 in the western English Channel), S2P3-R thus provides a means to test hypotheses regarding the sensitivity of 1-D biogeochemical processes to key model parameters, and/or to test the responses to variations of physical forcing on timescales ranging from diurnal to interannual, as noted in the final paragraph of the Discussion (lines 702-704).

The authors spend several pages describing the existing S2P3 model, which has already been published and is available online. The new methodology employed here appears to consist of modifying the source code so that it can run in a Unix environment and run at 5000-20000 grid points. Matlab plotting scripts are also provided. However, this in itself does not consist of a substantial advance in modeling science, or represent a particularly novel concept or idea.

Response: The description of S2P3 (Sect. 2.1) is a recap on more extensive details in Sharples (1999) and Sharples (2008), and actually includes some details on forcing that are specific to S2P3-R. This sub-section is intended to provide the necessary basic information on the model, for future users of S2P3-R. We disagree that the development of S2P3-R "does not consist a substantial advance", as only now can we routinely carry out multi-year simulations of physical and biological processes and structures at unprecedented temporal, vertical and horizontal resolution. We return to this issue in some of the responses below, but note here the evidence provided in new Fig. 11 and accompanying text (lines 647-654).

The primary issue I have with the manuscript, however is that the authors are essentially attempting to study 3D physical/biological shelf processes by ignoring advection. In many/ most shelf systems, advective processes play a critical role in controlling the distributions of nutrients and phytoplankton, and thus neglecting this key process is a major deficiency in the paper. Perhaps this may be why the observed chlorophyll concentrations (Fig. 4f) look nothing like the modeled chlorophyll concentrations (Fig. 4g)?

Response: While we agree that advective processes are of leading importance at some locations, 1D processes exert a first order control at many other locations (e.g., the northwestern North Sea, as emphasized by Sharples et al. 2006), and we might reasonably use S2P3-R accordingly and judiciously. We re-emphasize the key point that very high resolution is both appropriate and necessary for representing key 1D (vertical) processes and 2D

(horizontal) structures observed in shelf seas, such as tidal mixing fronts (lines 50-57). More complete 3D dynamical models cannot easily be deployed experimentally to investigate such processes and features (lines 637-646).

We respond more specifically to comments on the model-data comparison of Fig. 4: "Regarding structural discrepancy between observed chlorophyll concentrations in Fig. 4f and modeled chlorophyll concentrations in Fig. 4g, the northward-shifted surface maximum in the model is coincident with a more northward location of the tidal mixing front, which could be attributed to inadequacies in meteorological and/or tidal forcing." (lines 467-471). We do recognize that "The higher surface maximum of chlorophyll in the model may be in part due to neglected horizontal processes, such as along-front transports by a baroclinic jet supported by strong horizontal temperature gradients, and cross-frontal mixing processes associated with jet instability." (lines 471-474). However, "Higher chl-a concentrations in the model may alternatively be attributed to the relatively simple description of phytoplankton physiology, grazing and mobility (no sinking)." (474-476).

We reiterate that the model successfully reproduces key patterns in chl-a distributions with respect to physical structure (i.e., a SCM in the thermocline, increased surface chl-a at the front). Finally, in the concluding paragraph, we note that "Without *a priori* knowledge, the 1D approach is however valid for testing, against suitable observations of evolving physical structures, the extent to which advection may be important." (lines 696-698).

In addition, the S2P3-R implementation described here can take nearly a day to generate a year of 3D model results. Sophisticated community models including key physical processes lacking here (e.g. horizontal and vertical advection) as well as complete biogeochemical modules (rather than simply just phytoplankton and nutrient components) often take less than a day of run-time per year simulation for similar regional shelf applications. Because such commonly used models (e.g. the Regional Ocean Modeling System (ROMS)) include more key physical processes and take less time to run, it is not clear why the modeling framework described here (S2P3-R) is superior to (or even a logical alternative to) these existing and well-documented regional shelf community models.

Response: The quoted 1-day CPU demand is rather arbitrary, as S2P3-R can easily be run as a multi-processor job in separate domains. We have recently implemented S2P3-R in a larger western English Channel domain (3-9°W, 49-51°N) configured as twelve 1° × 1° sub-domains - see initial results in Fig. 11 in the revised manuscript and accompanying text (lines 647-654) - for an order of magnitude increase in speed of computation, and more sophisticated methods could be used to achieve much faster computation. We know of no other 1-km regional model of shelf sea physics and biology that is so easily configured and used experimentally. The UK Met Office continues to develop shelf sea models of increasing resolution (presently working on a 1-km model), but the high demands on human and computational resources preclude the wider community from undertaking such efforts (see also our response to Referee 1).

In summary, although I fully appreciate the utility of purely 1D models such as S2P3 for the purposes of scientific inquiry and as an instructional tool, the utility of implementing a 1D model regionally at 5000-20000 separate sites in an attempt to estimate 3D physical/ biological maps, while ignoring key 3D physical processes such as advection, is simply not clear.

Response: Ultimately, the S2P3-R framework is developed for use in suitable regions, where we know the shelf sea system to be dominated by 1D (vertical) processes, with horizontal processes dominated by tides and limited net horizontal transport. We clearly emphasize that model applications need to be carefully chosen and designed, bearing in mind the model framework. These perspectives are covered in the concluding paragraphs (lines 693-704).

However, the very fact that we are able to accurately reproduce monthly observations of thermal structure at E1 in the western English Channel over 2002-13 (see Fig. 6 of our revised manuscript), suggests that S2P3-R can be successfully used to investigate the wider region – from the seasonally stratified southern Celtic Sea to year-round mixed waters further to the east in the English Channel (see Fig. 11). We therefore consider there is much potential for S2P3-R to inform our fundamental understanding of physical and physiological controls on primary productivity across this wider region. The purpose of our manuscript is to document and establish the framework for these future investigations. These perspectives are covered in lines 655-663 of the revised Discussion.

1 **S2P3-R (v1.0): a framework for efficient regional modelling of physical and**

2 **biological structures and processes in shelf seas**

3

4 **Robert Marsh[1] Anna E. Hickman[1], and Jonathan Sharples[2,3]**

5

6 [1] University of Southampton, National Oceanography Centre, Southampton UK

7 [2] School of Environmental Sciences, University of Liverpool, Liverpool L69 3BX,

8 United Kingdom

9 [3] National Oceanography Centre, Liverpool, Joseph Proudman Building, 6 Brownlow

10 Street, Liverpool L3 5DA, UK

11

12 **Abstract**

13 An established 1-dimensional model of Shelf Sea Physics and Primary Production

14 (S2P3) is adapted for flexible use in selected regional settings over selected periods of

15 time. This Regional adaptation of S2P3, the S2P3-R framework (v1.0), can be

16 efficiently used to map 3-D physical and biological structures in shelf seas, in

17 particular the tidal mixing fronts that seasonally develop at boundaries between mixed

18 and stratified water. The model is highly versatile, deployed both as an investigative

19 research tool alongside more complex and computationally expensive models, and in

20 undergraduate oceanography modules and research projects, as a practical tool for

21 linking theory and field observations. Three different regional configurations of S2P3-

22 R are described and evaluated, illustrating a range of diagnostics, evaluated where

23 practical with observations. The model can be forced with daily meteorological

24 variables for any selected year in the reanalysis era (1948 onwards). Example

25 simulations illustrate the considerable extent of synoptic-to-interannual variability in

26 the physics and biology of shelf seas. In discussion, the present limitations of S2P3-R

27 are emphasized, and future model developments are outlined.

1. Introduction

In a global context, the shelf seas are disproportionately productive due to the continuous supply of nutrients (Holt et al., 2009a, and references therein). A variety of models have been developed to explore the processes that shape and maintain productivity. Such models necessarily couple physical and biological processes at high spatial resolution. Operational biogeochemistry and ecosystem models typically represent the system with relatively high complexity and are configured with the finest possible horizontal resolution, e.g., the 7 km Atlantic Margin Model NEMO-ERSEM (AMM7-NE) system (Edwards et al. 2012) – see also http://www.metoffice.gov.uk/research/news/marine-predictions. Such models may perform well alongside observations, but simulations rely on high performance computing resources such that extensive experimental work is consequently not practical.

In contrast to complex models, the Shelf Sea Physics and Primary Production (S2P3) model (Simpson and Sharples, 2012) exploits the dominance of vertical processes over horizontal processes in shelf seas. S2P3 explicitly represents vertical heat fluxes, vertical mixing of momentum, and vertical mixing of heat and tracers (nitrate and chl-a concentrations). Central to the model physics is a turbulence closure scheme, determining the light environment and nutrient fluxes that drive a simple primary production (nutrient-phytoplankton, or NP) model, such that phytoplankton growth responds to changes in stratification and mixing. In this way, S2P3 can efficiently simulate the seasonal cycle of stratification and primary production at a selected location, characterized by a local depth and tidal current amplitude. In particular, S2P3 has been used (e.g., Sharples 2008) to simulate idealized seasonal tidal mixing fronts (TMFs), analogous the observed discontinuities between mixed and seasonally stratified water in mid-latitude shelf seas (Simpson and Hunter 1974). While controlled to first order by vertical processes, the transition from mixed to stratified water across a TMF typically occurs on a horizontal scale of ~10-20 km (e.g., Moore et al., 2003), so for clear resolution of associated physical and biogeochemical structures, TMFs are ideally simulated at high horizontal resolution (1-2 km).

S2P3 was introduced as PHYTO-1D and originally described in Sharples (1999). An updated version of PHYTO-1D was described in Sharples (2008). The model is designed for use as an investigative (and educational) tool (see zipped material at

61   http://pcwww.liv.ac.uk/~jons/model.htm). S2P3 has been used as a research tool to

62   establish the varying influence of winds and air-sea heat fluxes on inter-annual

63   variability in the timing of stratification and the spring bloom in the northwestern

64   North Sea (Sharples et al. 2006), and to quantify the impact of spring-neap tidal

65   cycles on biological productivity at TMFs (Sharples 2008). In educational contexts,

66   S2P3 and forerunner models have been used for around 10 years in Year 3

67   undergraduate and masters level postgraduate teaching at the Universities of

68   Southampton and Liverpool, in the UK.

69   In spite of potential for widespread application, S2P3 has not been extensively used

70   and tested across real transects or in regions where 1D (vertical) processes are

71   dominant, such that the model can be appropriately used for investigating time-

72   evolving 3D structures. Introduced here, S2P3-R is a framework for using S2P3 to

73   efficiently model 3D physical and biological structures in shelf seas, for selected

74   years during the reanalysis era (Kalnay et al., 1996). The development of S2P3-R has

75   facilitated the simulation of 3-D structure in real time, for quick investigation of

76   ongoing changes and detailed fieldwork planning.

77   In the remainder of the paper, we first outline the S2P3-R framework. We start with a

78   brief description of the physical and biological components of S2P3, followed by

79   details of the modified source code, model performance and diagnostic options. This

80   is in turn followed by details on model setup in different domains (horizontal meshes

81   and tidal forcing), and the specification of meteorological forcing. We then evaluate

82   model simulations for four different regions, undertaken and diagnosed using the new

83   framework. In discussion, some important caveats are emphasized, and we outline the

84   prospects for development of S2P3 itself, within S2P3-R, to implicitly include lateral

85   processes that become influential near coasts and the shelf break and to resolve

86   variability in turbidity and phytoplankton physiology.

87

88   **2. The S2P3-R framework**

89   *2.1 S2P3*

90   Here, we provide a brief description of the physical and biological components of

91   S2P3, emphasizing key equations. For a more detailed model description, the reader is

92   referred to Sharples (1999) and Sharples (2008).

93

94 *2.1.1 Physical model*

95 Central to the physics of S2P3 is a turbulence closure scheme, for which the
96 prognostic variable is turbulent kinetic energy (TKE), formally defined as $q^2/2$, where
97 q is the turbulent intensity, or velocity scale (m s^{-1}). For a tidal current with x- and y-
98 components u and v, the tendency of TKE is expressed as

99

100
$$\frac{\partial}{\partial t}\left(\frac{q^2}{2}\right) = \frac{\partial}{\partial z}\left(K_q \frac{\partial}{\partial z}\left(\frac{q^2}{2}\right)\right) + N_z\left[\left(\frac{\partial u}{\partial z}\right)^2 + \left(\frac{\partial v}{\partial z}\right)^2\right] + K_z\left(\frac{g}{\rho}\frac{\partial \rho}{\partial z}\right) - \frac{q^3}{B_1 l}$$

(1)

101

102 where ρ is density, quadratic in temperature T (ρ = 1028.11 - 6.24956 × 10^{-2}T -
103 5.29468 × 10$^{-3}T^2$, assuming a constant salinity of 35.00), B_1 is a constant of the
104 closure scheme, K_q is the vertical eddy diffusivity for TKE, K_z is the vertical eddy
105 diffusivity for other scalar properties, N_z is vertical eddy viscosity, and l is an eddy
106 length-scale [$l = \kappa z(1 - z/h)^{0.5}$, at depth z, given total depth h and von Karmen's
107 constant κ = 0.41]. Forward time stepping is explicit throughout, with time-steps, Δt,
108 constrained by the diffusive stability criterion, $\Delta t < \Delta z^2/2N_z$, given depth intervals, Δz.
109

110 Tides and winds force the TKE profile for given boundary conditions:

111

112
$$q^2_{z=h} = B_1^{2/3}\frac{\tau_s}{\rho_{z=h}} \; ; \quad q^2_{z=0} = B_1^{2/3}\frac{\tau_b}{\rho_{z=0}}$$

(2a,b)

113

114 where τ_s is the surface ($z = h$) stress due to the wind, and τ_b is the near-bottom ($z = 0$)
115 stress due to tidal currents. The x- and y-components of wind stress are obtained as

116

117
$$\tau_{sx} = -c_d\rho_a u_w\sqrt{(u_w^2 + v_w^2)}; \quad \tau_{sy} = -c_d\rho_a v_w\sqrt{(u_w^2 + v_w^2)}$$

(3a,b)

118

119   given a drag coefficient c_d [$c_d = (0.75 + 0.067w) \times 10^{-3}$, for wind speed w], air density

120   ρ_a (= 1.3 kg m^{-3}), and u_w and v_w, the x- and y-components of wind. The x- and y-

121   components of near-bottom stress are obtained as

122

123
$$\tau_{bx} = -k_b\rho_0 u_1 \sqrt{(u_1^2 + v_1^2)}; \quad \tau_{by} = -k_b\rho_0 v_1 \sqrt{(u_1^2 + v_1^2)} \qquad \text{(4a,b)}$$

124

125   given a drag coefficient k_b (= 0.003), representative density for seawater ρ_0 (= 1025

126   kg m^{-3}), and u_1 and v_1, the x- and y-components of the current 1m above the seabed.

127   See Sharples (1999) for further details on the subsequent calculation of K_z, K_q and N_z.

128   In addition to mixing, the water column is locally heated and cooled. The tendency of

129   temperature, T, is obtained at each depth level as

130

131
$$\frac{\partial T}{\partial t} = \frac{\partial}{\partial z}\left(K_z \frac{\partial T}{\partial z}\right) + Q_h(z) \qquad \text{(5)}$$

132

133   where z is height above the seabed and $Q_h(z)$ is the net heating at depth z.

134   Heat fluxes are formulated as follows. We first define a surface net heat flux (Q_{net}) as

135   the sum of incoming shortwave radiation (Q_{SW}), long-wave back radiation (Q_{LW}), and

136   latent and sensible heat exchange with the atmosphere (Q_{sens} and Q_{lat}):

137

138
$$Q_{net} = Q_{SW} - (Q_{LW} + Q_{sens} + Q_{lat}) \qquad \text{(6)}$$

139

140   Incoming shortwave radiation, irradiance in the presence of clouds, is calculated as

141

142
$$Q_{SW} = (1.0 - 0.004C - 0.000038C^2)Q_{SW,c-s} \qquad \text{(7)}$$

143

144   where C is cloud fraction, and clear sky irradiance, $Q_{SW,c-s}$, is obtained as

145

146
$$Q_{SW,c-s} = S(1 - \alpha)f(\theta, t)(1 - \kappa_{SW}) \tag{8}$$

147

148 where S is the solar constant (= 1368 Wm^{-2}), α is an atmospheric albedo (= 0.24),

149 $f(\theta,t)$ is a function representing the daily and seasonal variation in day length at

150 latitude θ, and κ_{SW} is a short-wave absorption coefficient (= 0.06). Long-wave

151 radiation is calculated as

152

153
$$Q_{LW} = \varepsilon_{LW}(1.0 - 0.6{\times}10^{-4}C^2)(0.39 - 0.05q^{0.5})\sigma T^4 \tag{9}$$

154

155 where ε_{LW} is long-wave emissivity (= 0.985), q is vapour pressure ($q = Rq_s$, given

156 saturated vapour pressure $q_s(T)$ and relative humidity R), and σ is the Stefan-

157 Boltzmann constant ($\sigma = 5.67$ x 10^{-8} W m^{-2} K^{-4}). Sensible heat flux is calculated using

158 the bulk formula:

159

160
$$Q_{sens} = \rho_a c_p C_h U(T_s - T_a) \tag{10}$$

161

162 where c_p is the specific heat capacity of air (c_p = 1004 J kg^{-1} K^{-1}), C_h is a transfer

163 coefficient (C_h = 1.45 x 10^{-3}), U is surface wind speed, T_s is the sea surface

164 temperature, and T_a is surface air temperature. Latent heat flux is calculated using the

165 bulk formula:

166

167
$$Q_{lat} = \rho_a L_v C_e U(q_s - q) \tag{11}$$

168

169 where L_v is the specific heat capacity of air (L_v = 2.5 x 10^6 - 2.3 x $10^3 T_s$), and C_e is a

170 transfer coefficient (C_e = 1.5 x 10^{-3}).

171 The surface net heat flux is partitioned down the water column as follows. The red

172 end of the spectrum, 55% of shortwave radiation, is assumed to be absorbed at the top

173 depth level, hence the surface heating, $Q_{h,0}$ = 0.55Q_{SW} - (Q_{LW} + Q_{sens} + Q_{lat}). The

6

174   remaining 45% of insolation is available for heating at lower levels, distributed
175   exponentially throughout the water column as a heating rate $Q_h(z)$, according to

176

177
$$\frac{\partial Q_h}{\partial z} = -Q_h(z)\big(\lambda_0 + \varepsilon X_T(z)\big)$$
(12)

178

179   where λ_0 is an attenuation coefficient ($\lambda_0 = 0.1$ m^{-1}) and ε is a pigment absorption
180   cross-section ($\varepsilon = 0.012$ m^2 (mg chl)$^{-1}$), accounting for shading due to $X_T(z)$, the local
181   chlorophyll-a (chl-a) concentration (mg chl m^{-3}), taking $X_T(z) = q^{chl}P_C$, for cell chl-
182   a:carbon ratio, q^{chl} (0.03 mg chl (mg C)$^{-1}$), and carbon concentration, P_C (see below).
183

184   *2.1.2 Biological model*

185   Phytoplankton is modelled in terms of an equivalent carbon concentration (P_C, units
186   mg C m^{-3}) and internal cellular nitrogen (P_N). In each grid cell, P_C tendency is due to
187   the net effect of vertical mixing, growth and grazing, according to

188

189
$$\frac{\partial P_C}{\partial t} = \frac{\partial}{\partial z}\left(K_z \frac{\partial P_C}{\partial z}\right) + \mu P_C - G P_C$$
(13)

190

191   given a grazing impact rate G, and a growth rate, μ, that is a function of
192   photosynthetically-active radiation:

193

194
$$\mu = \mu_m\big(1 - e^{-(\alpha I_{PAR}\theta/\mu_m)}\big) - r^B$$
(14)

195

196   where α is the maximum quantum yield, I_{PAR} is the light availability, θ is the chl-
197   a:carbon ratio, r^B is the respiration rate, and the maximum growth rate, μ_m, is given by

198

199
$$\mu_m = 1.16\times10^{-5}\left(\frac{Q-Q_{sub}}{Q_m-Q_{sub}}\right)0.59e^{0.0633T}$$
(15)

200

201   where $Q = P_N/P_C$ is the cell nitrogen quota, Q_{sub} is the subsistence nutrient:carbon

202   quota, and Q_m is the maximum cell quota. The tendency for phytoplankton nitrogen

203   (P_N) is similarly described as

204

205
$$\frac{\partial P_N}{\partial t} = \frac{\partial}{\partial z}\left(K_z \frac{\partial P_N}{\partial z}\right) + uP_C - GP_N \tag{16}$$

206

207   where the uptake rate u is obtained as a Michaelis-Menton function of the dissolved

208   inorganic nitrogen concentration (DIN):

209

210
$$u = \left[u_m\left(1 - \frac{Q}{Q_m}\right)\frac{DIN}{(k_u + DIN)}\right] + \begin{cases}\mu Q, & \mu < 0 \\ 0, & \mu \geq 0\end{cases} \tag{17}$$

211

212   given k_u, a half saturation coefficient for nutrient uptake, and u_m, a maximum nutrient

213   uptake rate. The uptake of nitrogen leads to a tendency in dissolved inorganic nitrogen

214   (DIN):

215

216
$$\frac{\partial DIN}{\partial t} = \frac{\partial}{\partial z}\left(K_z \frac{\partial DIN}{\partial z}\right) - \mu P_C + eGP_N \tag{18}$$

217

218   where e is the fraction of grazed phytoplankton cellular nitrogen recycled

219   immediately back into the dissolved nitrogen pool.

220

221   Water column nitrogen is constantly restored towards an initial winter concentration,

222   DIN_0 (mmol m^{-3}), by a flux of inorganic nitrogen from the seabed:

223

224
$$\frac{\partial DIN_1}{\partial t} = \frac{f_{DIN}}{\Delta z}\left(1 - \frac{DIN_1}{DIN_0}\right) \tag{19}$$

225

226   where DIN_1 is the dissolved nitrogen in the bottom depth cell of the model grid, Δz

227   (m) is the thickness of the model grid cell, and f_{DIN} (mmol m^{-2} s^{-1}) is the maximum

228   flux of dissolved nitrogen from the seabed into the bottom depth cell.

229

230   The values of biological parameters (G, μ_m, θ, r^B, Q_{sub}, α, u_m, Q_m, k_u, e, DIN_0, f_{DIN}) are

231   as listed in Table I of Sharples (2008).

232

233   *2.2 Modified S2P3 source code, performance and diagnostics*

234   For the S2P3-R framework, we modified the Fortran 90 source code of S2P3 v7.0,

235   which includes additional commands and subroutines to facilitate the Winteracter

236   Fortran GUI toolset (Interactive Software Services Ltd., www.winteracter.com), the

237   model being supplied with a text book (Simpson and Sharples 2012) as an executable

238   application that runs under the Windows operating system. This source code was

239   modified for compilation and execution in a Unix environment by removing GUI-

240   related lines of code. These changes are solely to facilitate compilation and execution

241   in Unix environments, and S2P3 is thus far unchanged as a scientific tool.

242   Within the new framework, S2P3 can be used to generate geographically specific

243   maps, sections and time series, with varying run-time implications on a single

244   processor. Maps typically comprise 5000-20000 grid-points, while sections comprise

245   10-100 grid-points. For a given year (see below), maps can take over a day to

246   generate (depending on the extent of shallower water, where shorter time-steps are

247   necessary), while sections typically take a few minutes, and annual time series at a

248   single location typically take a few seconds.

249   Default mapped variables are presently limited to mid-summer surface-bottom

250   temperature difference, annual-mean surface heat flux, and annual net production,

251   although other quantities, such as the mid-summer sub-surface chl-a maximum

252   (SCM), have been mapped. The option for simulating sections is motivated by

253   opportunities for direct comparison with measurements obtained through surveys and

254   cruises. In selecting to simulate section data, constant depth intervals are specified for

255   plotting on a regular distance-depth mesh without the need for interpolation. The

256   option for time series at single locations is motivated by the availability of time series

257   at repeat Conductivity Temperature Depth (CTD) stations and moorings. Finally, we

258   save daily horizontal distributions of physical and biological variables for selected

259 periods, to generate animations that yield a range of insights not so easily appreciated
260 with individual maps or sections.

261 FORTRAN programmes are used to post-process model data for plotting, and
262 MATLAB scripts are used to plot model variables (as used to prepare the figures and
263 animations presented here). Example MATLAB plotting scripts are provided together
264 with the source code and other ancillary programmes and data files in s2p3-reg.zip
265 (see Section 5).

266

267 *2.3 Regional configurations*

268 Three domains have been developed and tested here, for reasons that are outlined in
269 turn. Figure 1 shows the bathymetry, while Table 1 specifies the boundaries,
270 resolution, tidal forcing and initial temperature field, for each domain. In an initial
271 stage of development, S2P3-R was developed for the northwest European shelf
272 domain. Development of the two other domains has been motivated by the extent to
273 which the different climatological and tidal forcing can be accommodated (in the shelf
274 seas around China) and by ongoing fieldwork (annual surveys south of Cornwall) in a
275 smaller region where the tidal mixing front is particularly sharp.

276 Bathymetry is typically in the range 50-100 m across most of the northwest European
277 shelf (Fig. 1a). However, some important details are emphasized for the other two
278 domains: a shallower inshore zone (depths < 30 m) in the Western English Channel
279 (Fig. 1b); a secondary shelf break (descending 50-100 m) in the East China Sea (Fig.
280 1c). At very high resolution, some artefacts of bathymetric surveying are apparent as
281 linear features in the bathymetry south of Cornwall (Fig. 1c).

282 For the northwest European shelf, bathymetry and current amplitudes for the leading
283 three tidal constituents (M2, S2, N2 - see Fig. S1 in Supplementary Material) were
284 obtained from the POLCOMS model (e.g., Holt et al. 2009b). For the Western
285 English Channel, bathymetry is extracted from the ETOPO1 global relief model
286 (Amante and Eakins, 2009) and tidal current amplitudes are interpolated from the
287 POLCOMS dataset. For the East China and Yellow Seas, current amplitudes for the
288 leading 13 tidal constituents were generated using OTPS (OSU Tidal Prediction
289 Software), based on the inverse method developed by Egbert et al. (1994) and Egbert
290 and Erofeeva (2002), and bathymetry is selected within the OTPS system. Opting to

291   use the leading five constituents for this region, S2P3 was adapted to include the two
292   diurnal constituents, O1 and K1, in addition to the semi-diurnal constituents S2, M2
293   and N2 (see Fig. S2).

294   One further distinction in regional setup concerns initial temperatures. At 1 January of
295   each year, the water column across the European shelf seas is presumed mixed
296   everywhere. In the default model, initial temperature is 10.1°C at all depths,
297   appropriate for the Celtic Sea. This initial temperature is also appropriate for the
298   Western English Channel, although we specify simulated 31 December temperatures
299   (constant through the fully mixed water column) for subsequent 1 January dates in the
300   case of simulations at the Western Channel Observatory (see Section 3.2). Elsewhere,
301   alternative values for initial temperature are appropriate, consistent with local climate.
302   Consider as an example the northeast sub-region of our northwest European shelf
303   domain. Sensitivity tests illustrate the importance of specifying an appropriate initial
304   temperature – see Fig. S3. If the initial temperature in this region is too high (Fig.
305   S3a), the net heat fluxes fall below -10 Wm^{-2} across much of the domain, especially to
306   the north (i.e., annual net cooling from a "warm start"), while if the temperature is too
307   low (Fig. S3b), heat fluxes exceed 10 Wm^{-2} at most locations (i.e., annual net
308   warming from a "cold start"). Only if the initial temperature is accurate to within
309   around 1°C do we avoid strong annual net cooling or heating (Fig. S3c). For the
310   China Seas, we specify a higher initial temperature of 15.1°C and simulate two
311   consecutive years, accounting for weak wintertime stratification in this region. We
312   analyse only the second year, for which more realistic initial conditions are thus
313   established across the wider domain (on 1 January of the second year).

314

315   *2.4 Meteorological forcing*

316   In addition to tidal mixing, S2P3 is forced with surface heat fluxes and wind stirring.
317   Heat is gained by shortwave radiation and lost via long-wave back-radiation, sensible
318   and latent heat fluxes - see Eqn. (6). Shortwave radiation varies with latitude and time
319   of year, and decreases with fractional cloud cover - see Eqns. (7) and (8). Long-wave
320   radiation varies with sea surface temperature and cloud cover – see Eqn. (9). Sensible
321   and latent heat losses vary with air temperature, wind speed and relative humidity
322   according to bulk formulae – see Eqns. (10) and (11).

323   Daily values for the four necessary meteorological variables are provided in a single
324   ASCII file. Sharples (2008) uses climatological meteorological data for the Celtic
325   Sea, while Sharples et al. (2006) use meteorological data for 1974-2003 from weather
326   stations in the vicinity of a study site in the northwestern North Sea. Here, we use
327   NCEP Reanalysis data provided by the NOAA/OAR/ESRL PSD, Boulder, Colorado,
328   USA, from their website at http://www.esrl.noaa.gov/psd/. These data are routinely
329   updated to within a day or so of the present time, and span the period from 1948. The
330   data is provided on a 2.5° global mesh, so each domain is forced everywhere with
331   meteorological data from a single 2.5° grid square, central to that region. Coordinates
332   of selected grid squares are listed in Table 1.

333   Figure 2 illustrates time series of meteorological variables for the three domains. In
334   initial testing, for the northwest European shelf, we use the "default" Celtic Sea
335   climatology (Sharples 2008). For the other two domains, data for 2013 are shown for
336   example. Note the extent of high-frequency synoptic variability in these cases, in
337   particular for relative humidity, cloud fraction and wind speed. Also note that the UK
338   spring of 2013 was exceptionally cold, hence air temperatures for the Western English
339   Channel sub-domain considerably below the Celtic Sea climatological average. Also
340   note considerable contrast between the maritime and continental climates, for the
341   European shelf and China Seas respectively.

342

343   **3. Model evaluation in the new framework**

344   *3.1 Northwest European shelf*

345   Figure 3 shows a summary of fields obtained for a simulation using the northwest
346   European shelf domain. Fig. 3a shows the annual-mean Hunter-Simpson parameter,
347   $\log_{10}(h/u^3)$, where h is the local depth and u is the amplitude of the local tidal current.
348   Previous studies (starting with Simpson and Hunter, 1974) have established a
349   threshold value of around 2.7, below (above) which the water column is well mixed
350   (stratified). $\text{Log}_{10}(h/u^3)$ is generally below 2.7 throughout the southern North Sea, and
351   across much of the eastern English Channel and the Irish Sea. These regions are
352   indeed well mixed throughout summer, as evident in near-zero surface-bottom
353   temperature differences for mid-July, shown in Fig. 3b. Elsewhere, stratification is
354   established, and the model hence simulates a set of fronts between mixed and

12

355 stratified water that are clearly observed in satellite data (see Fig. 8.1 in Simpson and

356 Sharples, 2012 - also indicated in Fig. 3a): the Islay front between Northern Ireland

357 and Scotland (A); the Western Irish Sea front enclosing a seasonally-stratified region

358 of the Irish Sea (B); part of the Cardigan Bay front (C); the St George's Channel front

359 between Wales and Ireland (D); the Ushant and Western English Channel front

360 between southwest England and Brittany, France (E). The model also simulates a

361 front observed between the seasonally-stratified northern North Sea and the

362 permanently mixed southern North Sea, including the Flamborough frontal system

363 (Hill et al. 1993, and references therein), also indicated (F) in Fig. 3a.

364 A limitation of the simulation presented in Fig. 3 is the use of default climatological

365 meteorological forcing, originally set up for simulating tidal mixing fronts in the

366 Celtic Sea. This has important consequences for local heat balances, evaluated here

367 with the annual-mean surface net heat flux, shown in Fig. 3c. In the central Celtic Sea

368 (south of Ireland), the net heat flux is slightly positive, in the range 0-5 Wm^{-2}.

369 Elsewhere, one might expect that a warmer (cooler) sea surface will lead to stronger

370 net heat loss (gain), via sensible and latent heat fluxes. However, the imbalance

371 reaches a maximum of 10 Wm^{-2} in the warm southwest English Channel (net heating)

372 and a minimum of -10 Wm^{-2} in the cool northern North Sea (net cooling). This is

373 consistent with insolation levels at these latitudes that are respectively higher and

374 lower than that for the Celtic Sea. Such imbalances are also a consequence of

375 specifying the same initial temperature everywhere (see section 2.2), such that the

376 northern North Sea is initially too warm (so must lose heat over the seasonal cycle),

377 and the southwest English Channel is initially too cool (so must gain heat). Net heat

378 fluxes are also notably positive in some regions that are well mixed all year round, in

379 particular the Irish Sea and parts of the English Channel. This is consistent with

380 enhanced heat storage due to mixing throughout the water column of heat gained in

381 summer (Simpson and Bowers 1984).

382 We have also experimented, on the northwest European shelf domain, with spatially

383 discriminate initial temperatures and meteorological forcing, the latter respecting

384 variation of NCEP reanalysis data (per 2.5° grid square) across the domain. While this

385 approach has the potential to restrict net heat fluxes closer to zero at all locations,

386 artefacts can be introduced to the forcing. This depends on how the NCEP data is

387 interpolated to the relatively fine 12-km mesh of S2P3-3D (not shown here).

13

388 Depending on temperature and the co-availability of photosynthetically active
389 radiation (PAR) and nutrients, the model simulates primary production. Annual net
390 carbon production per unit area is shown in Fig. 3d and simulated surface chl-a is
391 compared to satellite observations in Fig S4 and S5. The model reproduces key
392 aspects of the temporal and spatial variability in primary production and chl-a across
393 the shelf. Where aspects are not reproduced, we suggest (in Section 4) areas for future
394 model development.

395 Surface production rates (Fig 3d) and chl-a concentrations (Fig. S4) are especially
396 high in shallow coastal water that remains well mixed for most/all of the year, where
397 nutrients are consequently continuously re-supplied from the seabed, and PAR levels
398 are sufficient at all depths to maintain photosynthesis. We have limited confidence in
399 the simulated primary production and chl-a close to the coasts, for two specific
400 reasons. We presently do not account for the strong influence near many coasts of
401 freshwater (runoff), which has an important stratifying influence on the water column.
402 We also neglect the higher turbidity caused by non-algal particles that can reduce
403 PAR below a level necessary to sustain photosynthesis, e.g., where sediment loads are
404 relatively high in shallow regions of vigorous mixing, such as the southern North Sea.
405 Recognizing this model limitation, we choose not to plot model output in water
406 shallower than 30 m in Figs. 3 and S4.

407 Moving towards stratified regions, annual-mean carbon production rates generally
408 decline, although remain above 55 g C m^{-2} year^{-1} at most locations due to the
409 combined result of the major spring and minor autumn blooms (see below). This
410 decline is complemented by elevated productivity throughout summer at the
411 thermocline, associated with the development and persistence of the sub-surface chl-a
412 maximum (SCM). Primary production rates during the spring bloom (not shown)
413 reach 40 g C m^{-2} mon^{-1} or 1333 mg C m^{-2} d^{-1}, in line with observed magnitudes in the
414 order of 1000 mg C m^{-3} d^{-1} (Rees et al. 1999). Summertime chl-a and primary
415 production are low in the surface mixed layer, consistent with observed values of <1
416 mg chl-a m^{-3} and 5-30 mg C m^{-3} d^{-1}, respectively (Joint et al. 2000; Hickman et al.
417 2009). Simulated surface chl-a concentrations are broadly consistent with satellite
418 observations, although values are typically double those observed (see Figs. S4 and
419 S5). The model does not reproduce the enhanced primary production and chl-a
420 observed in the surface at the Celtic Sea shelf break (e.g., compare Figs. S4 and S5,

421 for April and May), because it does not include specific physical processes, such as

422 the internal tide, that are important for vertical nutrient supply to the surface in these

423 regions (Sharples et al. 2007).

424 Following the spring bloom, surface productivity and surface chl-a concentrations

425 remain elevated (above background values) near three tidal mixing fronts in particular

426 – the Ushant and Western English Channel front, the Islay front, and the St George's

427 Channel front – for June-September in the simulation (Fig. S4) and for May-July in

428 the observations (Fig. S5). Surface chl-a concentrations decline towards more

429 stratified waters, coincident with deepening of the SCM away from fronts and

430 associated zones of spring-neap frontal adjustment (Pingree et al. 1978, Weston et al.

431 2005, Hickman et al. 2012). At the Ushant Front, predicted peak July primary

432 production of 80-100 mg C m^{-3} d^{-1} is considerably smaller than in situ measurements

433 of 59-126 mg C m^{-3} h^{-1} (implying daily production of around 1000 mg m^{-3} d^{-1}), for

434 surface waters at a frontal station in late July (Holligan et al. 1984). However, the

435 model estimates are intermediate between corresponding surface observations for

436 mixed and stratified waters (reported in Holligan et al. 1984), emphasizing the very

437 localized character of frontal productivity, which is not easily captured with our

438 relatively coarse model resolution (here around 12 km) and in the absence of

439 horizontal processes that may lead to convergence of material at the front.

440 In the southern Irish Sea and south of the Islay front, simulated surface chl-a

441 concentrations are notably very low, at around 0.1 mg chl-a m^{-3} (see Fig. S4). These

442 low values are found in regions where the tidal current amplitude is especially strong

443 (see Fig. S1) in water that is sufficiently deep (~100 m, see Fig. 1a) for PAR to fall

444 below a threshold value within the well-mixed water column (Fig. 3b). So in spite of

445 very high nutrient levels throughout the year (not shown), light is a severe limitation

446 on photosynthesis and hence productivity. This aspect of the simulation is inconsistent

447 with surface chl-a concentrations of around 1 mg chl-a m^{-3} observed in this region

448 (Fig. S5; Pemberton et al. 2004; Moore et al. 2006). A likely explanation is that the

449 model does not resolve photo-acclimation, the known ability of phytoplankton to

450 acclimate to ambient light conditions (e.g. Geider et al. 1997), and so does not resolve

451 the photo-physiological differences between stratified and mixed water columns

452 (Moore et al. 2006). Dissolved inorganic nitrate (DIN) concentrations in the northwest

453 European shelf region during winter and in the bottom mixed layer during summer

15

454 (not shown) are 5-6 mmol m^{-3}, consistent with observed values around 6-9 mmol m^{-3}

455 (Joint et al. 2001; Hickman et al. 2012).

456 To illustrate typical vertical structure across a mid-summer tidal mixing front, Figure

457 4 shows observations and corresponding simulations for day 215 (3 August) of 2003,

458 along a section through the Celtic Sea front (Fig. 4a), located at around 52°N. The

459 temperature structure (Fig. 4b,c) illustrates stratified water south of 52°N, with mixed

460 water to the north. DIN concentrations are high in mixed water and in the lower layer

461 of the stratified water, and depleted in the surface layer of the stratified water (Fig.

462 4d,e). Chl-a concentrations reach a surface maximum at the front, with elevated

463 values extending southwards in the model - the SCM supported by a weak diffusive

464 DIN flux across the thermocline (Fig. 4f,g).

465 In broad terms, the model reproduces the observations, although the mixed water is

466 about 1°C cooler than observed, and DIN and chl-a concentrations are about 50%

467 higher at most depths. Regarding structural discrepancy between observed chl-a

468 concentrations in Fig. 4f and modeled chl-a concentrations in Fig. 4g, the northward-

469 shifted surface maximum in the model is coincident with a more northward location

470 of the tidal mixing front, which could be attributed to inadequacies in meteorological

471 and/or tidal forcing. The higher surface maximum of chl-a in the model may be in part

472 due to neglected horizontal processes, such as along-front transports by a baroclinic

473 jet supported by strong horizontal temperature gradients, and cross-frontal mixing

474 processes associated with jet instability. Higher chl-a concentrations in the model may

475 alternatively be attributed to the relatively simple description of phytoplankton

476 physiology, grazing and mobility (no sinking).

477

478 *3.2 Western English Channel*

479 For 1 May to 7 October of 2013, selected daily model fields are saved and animated

480 (see Supplementary Material Part B, "Example Animation", and accompanying

481 commentary text). A wide range of phenomena are evident in the animation, including

482 the earliest establishment of stratification during May, expressed as a surface-bottom

483 temperature difference, and the rapid uptake of surface DIN, which declines to near-

484 zero concentrations with the development of a spring bloom (high surface chl-a

485 levels) that peaks in early-mid June. We note that the exceptionally cold spring of

486   2013 substantially delayed the onset of stratification and the spring bloom (also

487   suggested by satellite data – not shown). The spring-neap cycle of stronger mixing (on

488   spring tides) and strengthened stratification (on neap tides) causes ~14-day "beating"

489   of chl-a concentration, between low values on spring tides and high values on neap

490   tides, most notably at the front between inshore mixed and offshore stratified waters

491   off southwest Cornwall throughout June and July.

492   To illustrate the interannual variability of summer stratification, Figure 5 shows

493   surface-bottom temperature differences on day 190 (8 or 9 July) of 2002-13. The

494   region is characterized by mixed water to the northwest associated with locally strong

495   tidal current amplitudes (see Fig. S1), and stratified water to the southwest (where

496   tides are weaker), with a secondary area of stratification centred around 4.5° W 50.1°

497   N (coincident with a local minimum in tidal current amplitude). The water column

498   remains mixed all year round in shallow water close to the coast, at most locations

499   and in most years. A complex arrangement of mixed and stratified water is simulated

500   in the northeast of the region, associated with highly variable bathymetry (see Fig.

501   1c). When a cold spring is followed by a warm summer (e.g., 2006, 2010, 2013),

502   stratification is particularly strong, with surface-bottom temperature differences

503   reaching almost 7°C in the southwest of the region.

504   To locally validate the simulation, we use observations at L4 (50° 15.00' N, 4° 13.02'

505   W) and E1 (50° 02.00' N, 4° 22.00' W), hydrographic stations that have been occupied

506   weekly and monthly, respectively, as part of the Western Channel Observatory

507   (http://www.westernchannelobservatory.org.uk/data.php). Here, seasonal cycles of

508   stratification and phytoplankton dynamics have been extensively studied (Smyth et al.

509   2010). In Fig. 5, we over-plot observed temperature differences for station

510   occupations within a few days (L4) or 1-2 weeks (E1) of day 190. Observed

511   differences are generally indistinguishable from the simulated differences.

512   For a more comprehensive validation, Figure 6 shows time series of surface-bottom

513   temperature differences observed and (daily) simulated at L4 and E1. The temperature

514   at the depth of the maximum chl-a concentration is also plotted at E1, confirming the

515   existence of an SCM within the seasonal thermocline. Starting on 1 January 2002, we

516   simulate one year at a time, specifying a mixed water column temperature on, e.g., 1

517   January 2003 with the corresponding temperature on 31 December 2002, etc. This

518   ensures continuity in temperatures between years, respecting a small degree of

519   interannual variability in wintertime temperature at L4 and E1. Weak stratification
520   (maximum ~4°C) typically is established over ~5 months of each summer at L4,
521   while stronger stratification (up to ~7°C) develops for longer (by 1-2 months) at E1.
522   Model-observation agreement is remarkably good, with close correspondence
523   between not just surface temperatures, but also bottom temperatures. The seasonally
524   varying stratification at both stations is generally reproduced to within 1°C, although
525   high-frequency extremes are under-sampled by weekly (monthly) occupations of L4
526   (E1), and there is more disagreement at L4. This is most likely because the water
527   column at L4 is strongly influenced by freshwater, with low surface salinity having a
528   substantial effect on stratification.

529   Vertical salinity structure also explains the apparent temperature instability (negative
530   surface-bottom temperature differences) observed at L4 in winter - the water column
531   is in fact statically stable throughout the time series. The addition of salinity as a
532   model state variable, and first order representation of the coastal freshwater influence,
533   would likely improve the simulation of temperature variability at L4 - we return to
534   this issue in the Discussion.

535   With some confidence in model performance, in Figure 7 we show temperature, DIN
536   and chl-a in sections through the developing tidal mixing front east of Lizard
537   peninsula, along 50.017°N, on days 100, 130, 160 and 190 of 2013. We select this
538   section as representative of CTD transects undertaken annually in late June/early July
539   by University of Southampton fieldwork students. On day 100 (early April), the water
540   column is well mixed almost everywhere, with very weak stratification in temperature
541   evident at 10 km along the section. DIN concentrations are high (~6 mmol m^{-3})
542   throughout the water column for bottom depths exceeding a threshold value (~40 m),
543   below which PAR falls below a critical value within the water column. As bottom
544   depths become shallower (progressing inshore), DIN concentrations rapidly fall to
545   near zero, where PAR is sufficient at all depths to sustain plankton growth and
546   associated DIN uptake in the model. Inshore chl-a concentrations are accordingly high
547   (12-13 mg chl-a m^{-3}), falling rapidly with distance to background values (~0.1 mg
548   chl-a m^{-3}) offshore.

549   By day 130 (early May), the water remains well mixed, although warmer by 1-2°C,
550   and high productivity has spread offshore, presumably due to intermittent weak
551   stratification during preceding days. By day 160, stratification is clearly established

18

552 beyond 4 km offshore. DIN concentrations are now reduced to near-zero in the upper

553 20 m of the stratified water, and high chl-a concentrations are evidence of the spring

554 bloom. By day 190, stratification has strengthened and DIN concentrations in the deep

555 layer of stratified water columns are further depleted through vertical mixing with the

556 upper photic zone, although surface chl-a concentrations have by this time

557 substantially declined in the upper layer. The boundary between mixed and stratified

558 waters on days 160 and 190 marks the position of the tidal mixing front. The model

559 has been further used to evaluate the extent of interannual variability around the time

560 of annual fieldwork, in the third week of June. Temperature sections on day 169 of

561 2002-13 (see Figure S6) reveal a wide range of offshore stratification and frontal

562 structure in recent years, with strongest stratification in 2010, weakest stratification in

563 2011, and a most clearly defined front in 2009.

564 As an example of the seasonal cycles in temperature, surface DIN and surface chl-a at

565 four locations across the front (spanning the distance range 3-7 km in Fig. S6), Figure

566 8 shows evolution of these variables through 2013. Stratification is very marginal and

567 intermittent at 5.033°W, with surface-bottom temperature differences occasionally

568 reaching 2°C. DIN concentrations fall close to zero over days 130-300 and chl-a

569 concentrations are high (in the range 6-8 mg chl-a m^{-3} throughout this period. Related

570 to the intermittent stratification are similar fluctuations in chl-a. This variability is in

571 part attributed to the near-fortnightly spring-neap tidal cycle, which leads to periodic

572 replenishment of nutrients, out of phase with more favourable PAR regimes.

573 Progressing offshore into deeper water, the seasonal cycle transforms towards

574 stronger stratification, a shorter period of surface DIN reduction, and a stronger peak

575 in surface chl-a around day 150 that corresponds to the spring bloom, followed by

576 substantially lower concentrations during the rest of summer.

577

578 *3.3 East China and Yellow Seas*

579 Figure 9 shows example fields for a simulation using the East China Sea and Yellow

580 Sea domain with 2013 forcing. Fig. 9a shows the annual-mean Hunter-Simpson

581 parameter, $\log_{10}(h/u^3)$, which falls below 2.7 in particularly shallow regions (see Fig.

582 1d) that are also characterized by high amplitude tidal currents (see Fig. S2).

583 $\text{Log}_{10}(h/u^3)$ conversely exceeds 5.0 in the isolated Bohai Sea, lying to the northwest of

584   the Yellow Sea. As for the northwest European shelf, regions with $\log_{10}(h/u^3) < 2.7$
585   remain well mixed throughout summer (Fig. 9b). Elsewhere, stratification is stronger
586   than for the northwest European shelf, with surface-bottom temperature differences
587   on day 190 of ~10°C across much of the stratified shelf. A major feature of Fig. 9b is
588   the front between mixed and stratified water in the East China Sea that is clearly
589   observed in satellite SST data (Hickox et al. 2000). The simulations also capture the
590   complex system of fronts observed in the Taiwan Strait (Zhu et al. 2013).

591   The specification of common meteorological variables across ~20° of latitude and
592   ~15° of longitude is a considerable approximation, and the annual-mean net surface
593   heat flux field is an important measure of resulting heat imbalances (Fig. 9c). We
594   regard these values as not too excessive, ranging from around 5 Wm^{-2} (heat gain) in
595   the far south to around -10 Wm^{-2} (excess heat loss) in the far north (Bohai Sea).
596   Annual-mean carbon production rates in the well-mixed shallow regions of the East
597   China Sea range from 300 to 450 g C m^{-2} $year^{-1}$, falling to ~100 g C m^{-2} $year^{-1}$ in the
598   more extensive stratified region (Fig. 9d). These predictions are similar in magnitude
599   to estimates of primary production based on in situ observations (e.g., 145 g C m^{-2}
600   $year^{-1}$ for "the entire shelf of the East China Sea", Gong et al. 2003). Monthly-mean
601   surface chl-a distributions are broadly comparable to satellite observations, although
602   maximum model chl-a concentrations are generally double those observed, and the
603   spring bloom is ~1 month late, in May rather than April (e.g., for 2013, Figs. S7 and
604   S8). Discrepancies between the model and observations in this region would also be
605   improved by model developments relating to horizontal advection and turbidity close
606   to the coast and to photo-physiology, as described for the northwest European shelf.

607   To complete the three-dimensional picture, Figure 10 shows show temperature, DIN
608   and chl-a concentration in sections through the developing front of the central East
609   China Sea, along 32°N, on days 100, 130, 160 and 190 of 2013. Bottom depth
610   increases considerably with distance offshore. In water of depth < 40 m, the water
611   column remains well-mixed throughout the year, while in deeper water, stratification
612   becomes established between days 100 and 130. In stratified water, DIN is already
613   depleted in the surface layer over days 100-130, and is gradually further depleted in
614   the lower layer over days 130-190 through progressive mixing into the photic zone. A
615   local surface maximum in chl-a concentration is evident at the frontal boundary (~250

km) on day 130, while a SCM is evident in stratified water on days 160 and 190. The SCM is most clearly defined at ~25 m on day 190.

4. Summary and discussion

We have developed S2P3-R, a versatile framework for efficient modeling of physical and biological structures and processes in shelf seas, adopting an existing 1-D model, S2P3. Here, we compliment ongoing development and use of the 1-D model for specific research hypotheses (e.g., Bauer and Waniek 2013) and in educational settings, where idealized simulations (e.g., Sharples 2008) are linked to realistic situations such as fieldwork contexts (e.g., off Cornwall). The realism of S2P3-R is predicated on our understanding that 1D (vertical) processes dominate 2D (horizontal) processes across much of the shelf seas, where we have the observations necessary for a co-evaluation of these processes. Where appropriate, the framework facilitates experiments to investigate the sensitivity of measurable quantities (e.g., chl-a concentration) to a wide range of physical and biological processes that can be adjusted with corresponding model parameters. Where high quality observations are available (e.g., at E1 in the western English Channel), S2P3-R thus provides a means for improving our fundamental understanding of the system. With tuned parameters, S2P3-R furthermore provides the means to carry out credible multi-year simulations of physical and biological processes and structures at unprecedented temporal, vertical and horizontal resolution.

At the seasonal timescale, the most striking 3D features are tidal mixing fronts (TMFs). Realistic representation of TMFs, demanding high horizontal resolution, amounts to first-order evaluation of any simulation, e.g., the UK Met Office forecast system (O'Dea et al., 2012), which has the same relatively coarse (12 km) resolution as our northwest European shelf domain. The summer surface-bottom temperature differences across the northwest European shelf and the associated TMFs in S2P3-R (Fig. 3a) compare well with the 3D model results (O'Dea et al. 2012, their Fig. 10). Our simpler approach thus indicates the importance of 1-D processes in forming these features, the locations of which are consistent with these more complex (hence expensive) models that cannot so easily be deployed experimentally.

647   It is natural to deploy S2P3 across multiple processors, with sub-domains computed
648   independently in parallel. This has been trialled for twelve $1° \times 1°$ sub-domains across
649   the southern Celtic Sea and western English Channel at a resolution of 1 km,
650   substantially expanding our Western English Channel domain with essentially no
651   extra computational expense. Figure 11 shows the July surface-bed temperature
652   difference across this region, illustrating how we are able to efficiently simulate
653   regional stratification at unprecedented horizontal resolution. Massively parallel
654   computing would of course reduce compute time by several orders of magnitude.

655   We have evaluated the model in various ways with available observations,
656   specifically addressing spatial patterns, vertical structures, and seasonal-interannual
657   variability. 3D temperature structures are reproduced with considerable success, as are
658   key aspects of the spatial and temporal variability in nutrient and chl-a concentrations.
659   In particular, we are able to accurately reproduce monthly observations of thermal
660   structure at E1 in the western English Channel over 2002-13 (Fig. 6), providing
661   confidence in the use of S2P3-R in this region. We therefore consider there is much
662   potential for S2P3-R to investigate physical and physiological controls on primary
663   productivity at regional scales.

664   Elsewhere, differences between the model and observations are informative because,
665   for example, they identify regions in which processes other than those currently
666   represented in the model are important. In particular, we note several processes
667   specific to coasts and shelf breaks, of relevance to several physical aspects of the
668   domains considered here:

669   • The coastal zone around Cornwall, typified by station L4, is strongly
670   influenced by riverine inputs that promote surface freshening and stratification
671   and alter light attenuation by non-algal particles and dissolved organic matter
672   (Groom et al., 2009; Smyth et al., 2010)
673   • The northern North Sea is strongly influenced by shelf edge exchange that
674   leads to the inflow of relatively warm and salty Atlantic Water (Huthnance et
675   al., 2009)
676   • The Yangtze River and two branches of the Kuro Shio - the Taiwan Current
677   and the Tsushima Warm Current - exert strong influences on stratification and
678   productivity in the East China Sea (e.g., Son et al., 2006).

679 In future versions of S2P3-R, a number of corresponding enhancements are therefore
680 planned:

- Implicit divergence of large-scale horizontal heat and tracer transport,
  particularly important near shelf breaks (e.g., northern North Sea)

- Addition of salinity as a state variable, followed by the implicit representation
  of horizontal salinity gradients associated with coastal runoff

- Locally enhanced background turbidity associated with coastal runoff and/or
  shallow water depths

687 Further development will formally establish the (presently prototype) option to
688 prescribe spatially variable initial temperatures and meteorological variables,
689 interpolated appropriately to each model mesh. As an additional diagnostic, the
690 thermal wind balance may be used with the 3-D density field to infer the residual
691 flows that are associated with TMFs (e.g., Hill et al., 2008), indicating the potential
692 importance of net advection.

693 We reiterate that the S2P3-R framework is developed specifically for use in suitable
694 regions, where the shelf sea system is controlled to first order by 1D (vertical)
695 processes, with horizontal processes dominated by tides, and limited net horizontal
696 transport. Without *a priori* knowledge, when tested against suitable observations of
697 evolving physical structures, the 1D approach informs on the extent to which
698 advection may be important. Model experiments should be carefully chosen and
699 designed, bearing in mind current 1D limitations and simplifications of S2P3-R.

700 In summary, the S2P3-R framework (v1.0) provides the flexibility to undertake
701 research experiments in finely-resolved realistic domains where 1-D processes
702 dominate, to test hypotheses regarding the sensitivity of 1-D biogeochemical
703 processes to key model parameters, and/or to test the responses to variations of
704 physical forcing on timescales ranging from diurnal to interannual. Combining
705 flexibility with computational efficiency, the S2P3-R framework may further
706 contribute to capacity building in marine monitoring and management for
707 individuals/organisations without the resources to run or analyse complex models of
708 their territorial waters or exclusive economic zones.

709

Code availability

The S2P3-R (v1.0) framework, comprising source code along with example scripts and output, is available online from:

`ftp://ftp.noc.soton.ac.uk/pub/rma/s2p3-reg.tar.gz`

Unzipped and uncompressed, the directory `/s2p3_reg_v1` contains several sub-directories:

- `/main` contains the source code, `s2p3v7_reg_v1.f90`, which is compiled "stand-alone", and executed using accompanying scripts, with examples of "map" (the northwest European Shelf simulation, as Fig. 3), "section" (Celtic Sea) and "time series" (E1) simulations (`run_map`, `run_section` and `run_timeseries`, respectively)
- `/domain` contains bathymetry and tide data for the northwest European Shelf region (`s12_m2_s2_n2_h_map.asc`), for a selected north-south section in the Celtic Sea (`s12_m2_s2_n2_h_sec.asc`) and for a selected point, E1 in the western English Channel (`s12_m2_s2_n2_h_tim.asc`)
- `/met` contains climatological meteorological forcing (`Celtic_met.dat`)
- `/output` contains example output data from the three runs (map, section, time series)
- `/plotting` contains MATLAB scripts for plotting maps, sections and time series (`plot_map`, `plot_section` and `plot_timeseries`, respectively)

The ancillary files needed for simulations in the domains "Western English Channel" and "East China and Yellow Seas", and for a selection of years, are available on request from the author (e-mail rm12@soton.ac.uk).

24

745

746 **References**

747

748 Amante, C. and B. W. Eakins (2009). ETOPO1 1 Arc-Minute Global Relief Model:
749   Procedures, Data Sources and Analysis. NOAA Technical Memorandum
750   NESDIS NGDC-24, 19 pp.

751

752 Bauer, A., and J. J. Waniek (2013). Factors affecting the chlorophyll a concentration
753   in the central Beibu Gulf, South China Sea, *Mar. Ecol. Prog. Ser.*, **474**, 67-88,
754   doi:103354/meps10075

755

756 Edwards, K. P., Barciela, R., and M. Butenschön (2012). Validation of the NEMO-
757   ERSEM operational ecosystem model for the North West European Continental
758   Shelf, *Ocean Sci.*, **8**, 983-1000, doi:10.5194/os-8-983-2012.

759

760 Egbert, G. D., Bennett, A. F., and M. G. G. Foreman (1994). TOPEX/POSEIDON
761   tides estimated using a global inverse model. *J. Geophys. Res.*, **99**, 24821-
762   24852, doi:10.1029/94JC01894

763

764 Egbert, G. D., and S. Y. Erofeeva (2002). Efficient Inverse Modeling of Barotropic
765   Ocean Tides. *J. Atmos. Oceanic Technol.*, **19**, 183–204. doi:
766   http://dx.doi.org/10.1175/1520-0426(2002)019<0183:EIMOBO>2.0.CO;2

767

768 Geider, R. J., MacIntyre, H. L., and T. M. Kana (1997). A dynamic model of
769   phytoplankton growth and acclimation: responses of the balanced growth rate
770   and chlorophyll a:carbon ratio to light, nutrient-limitation and
771   temperature. *Mar. Ecol. Prog. Ser.*, **148**, 187-200.

772

773 Gong, G.-C., Wen, Y.-H., Wang, B.-W., and G.-J. Liu (2003). Seasonal variation of
774   chlorophyll a concentration, primary production and environmental conditions
775   in the subtropical East China Sea. *Deep-Sea Research II*, **50**, 1219–1236,
776

777 Groom, S., Martinez-Vicente, V., Fishwick, J., Tilstone, G., Moore, G., Smyth, T.,
778   and D. Harbour (2009). The Western English Channel Observatory: optical
779   characteristics of station L4. *J. Mar. Sys.*, **77**, 278-295.
780

781 Hickman, A. E., Holligan, P. M., Moore, C. M., Sharples, J., Krivtsov, V. and M. R.
782   Palmer (2009). Distribution and chromatic adaptation of phytoplankton within a
783   shelf sea thermocline. *Limnol. Oceanogr.*, **54**, 525-536.
784

785 Hickman, A. E., Moore, C. M., Sharples, J., Lucas, M. I., Tilstone, G. H., Krivtsov, V.
786   and P. M. Holligan (2012). Primary production and nitrate uptake within the
787   seasonal thermocline of a stratified shelf sea. *Mar. Ecol. Prog. Ser.*, **463**, 39-57,
788   doi:10.3354/meps09836
789

790 Hickox R., I. Belkin, P. Cornillon and Z. Shan (2000). Climatology and Seasonal
791   Variability of Ocean Fronts in the East China, Yellow and Bohai Seas from
792   Satellite SST Data. *Geophy.* Res. Lett., **27**, 2945-2948.
793

794 Hill, A. E., James, I. D., Linden, P. F., Matthews, J. P., Prandle, D., Simpson, J. H.,
795   Gmitrowicz, E. M., Smeed, D. A., Lwiza, K. M. M., Durazo, R., Fox, A. D., and
796   D. G. Bowers (1993). Dynamics of tidal mixing fronts in the North Sea [and
797   discussion]. *Phil. Trans. Roy. Soc. Lond. (A)*, **343**, 1669 (1993): 431-446.
798

799 Hill, A. E., J. Brown, L. Fernand, J. Holt, K. J. Horsburgh, R. Proctor, R. Raine, and
800   W. R. Turrell (2008). Thermohaline circulation of shallow tidal seas. *Geophys.*
801   *Res. Lett.*, **35**, L11605, doi:10.1029/2008GL033459.
802

803 Holligan P. M., Williams, P. J. L., Purdie, D., and R. P. Harris (1984) Photosynthesis,
804   respiration and nitrogen supply of plankton populations in stratified, frontal and
805   tidally mixed shelf waters. *Mar. Ecol. Prog. Ser.*, **17**, 201–213.
806

807   Holt, J., Harle, J., Proctor, R., Michel, S., Ashworth, M., Batstone, C., Allen, I.,
808   Holmes, R., Smyth, T., Haines, K., Bretherton, D., and G. Smith (2009).
809   Modelling the global coastal ocean. *Phil. Trans. Roy. Soc. A*, **367**, 939-951, doi:
810   10.1098/rsta.2008.0210

811

812   Holt, J., Wakelin, S., and J. Huthnance (2009). Down-welling circulation of the
813   northwest European continental shelf:,A driving mechanism for the continental
814   shelf carbon pump. *Geophys. Res. Lett.*, **36**, L14602,
815   doi:10.1029/2009GL038997

816

817   Huthnance, J. M., Holt, J. T., and S. L.Wakelin (2009). Deep ocean exchange with
818   west-European shelf seas. *Ocean Sci.*, **5**, 621–634, www.ocean-
819   sci.net/5/621/2009/

820

821   Joint, I., and S. B. Groom (2000). Estimation of phytoplankton production from
822   space: current status and future potential of satellite remote sensing. *J. Exp.*
823   *Mar. Biol. Ecol.*, **250**, 233-255.

824

825   Kalnay, E., Kanamitsu. M., and R. Kistler (1996). The NCEP/NCAR 40-year
826   reanalysis project, *Bull. Amer. Meteor. Soc.*, **77**, 437-470.

827

828   Moore, C. M., Suggett, D. J., Hickman, A. E., Kim, Y. N., Tweddle, J. F., Sharples,
829   J., Geider, R. J. and P. M. Holligan (2006). Phytoplankton photoacclimation and
830   photoadaptation in response to environmental gradients in a shelf sea. *Limnol.*
831   *Oceanogr.*, **51**, 936-949.

832

833   Moore, C. M., Suggett, D., Holligan, P. M., Sharples, J., Abraham, E. R., Lucas, M.
834   I., Rippeth, T. P., Fisher, N. R., Simpson, J. H., and D. J. Hydes (2003).
835   Physical controls on phytoplankton physiology and production at a shelf sea
836   front: a fast repetition-rate fluorometer based field study *Mar. Ecol. Prog. Ser.*,
837   **259**, 29–45.

838

839   O'Dea, E. J., Arnold, A. K., Edwards, K. P., Furner, R., Hyder, P., Martin, M. J.,
840   Siddom, J. R., Storkey, D., While, J., Holt, J. T., and H. Liu (2012). An

841   operational ocean forecast system incorporating NEMO and SST data
842   assimilation for the tidally driven European North-West shelf. *Journal of*
843   *Operational Oceanography*, 5 (1). 3-17.

844

845   Pemberton, K., Rees, A. P., Miller, P. I., Raine, R., and I. Joint (2004). The influence
846   of water body characteristics on phytoplankton diversity and production in the
847   Celtic Sea. *Cont. Shelf Res.*, **24**, 2011–2028.

848

849   Pingree, R., Holligan, P., and G. T. Mardell (1978). The effects of vertical stability on
850   phytoplankton distributions in the summer on the northwest European Shelf.
851   *Deep Sea Res.*, **25**, 1011–1028.

852

853   Rees, A. P., Joint, I., and K. M. Donald (1999). Early spring bloom phytoplankton-
854   nutrient dynamics at the Celtic Sea Shelf Edge. *Deep Sea Research II*, **46**, 483–
855   510.

856

857   Sharples, J., (1999). Investigating the seasonal vertical structure of phytoplankton in
858   shelf seas. *Marine Models Online.* **1**, 3-38.

859

860   Sharples, J., Ross O.N., Scott, B.E., Greenstreet, S., Fraser, H. (2006). Inter-annual
861   variability in the timing of stratification and the spring bloom in the North-
862   western North Sea. *Cont. Shelf Res.*, **26**, 733-751.

863

864   Sharples, J., Tweddle, J. F., Green, J. A. M., Palmer, M. R., Kim, Y.-N., Hickman, A.
865   E., Holligan, P. M., Moore, C. M., Rippeth, T. P., Simpson, J. H., and V.
866   Krivtsov (2007). Spring-neap modulation of internal tide mixing and vertical
867   nitrate fluxes at a shelf edge in summer. *Limnol. Oceanogr.*, 52, 1735-1747.

868

869   Sharples, J. (2008). Potential impacts of the spring-neap tidal cycle on shelf sea
870   primary production. *Journal of Plankton Research*, **30**, 183-197.

871

872   Simpson, J. H., and J. R. Hunter (1974). Fronts in the Irish Sea. *Nature*, **250**, 404-406.

873

874   Simpson, J. H., and D. G. Bowers (1984). Geographical variations in the seasonal
875   heating cycle in northwest European shelf seas. *Annales Geophysicae*, **2**(4),
876   411-416.
877

878   Simpson, J. H., and J. Sharples (2012). *Introduction to the Physical and Biological*
879   *Oceanography of Shelf Seas*. Cambridge University Press.
880

881   Smyth, T. J., Fishwick, J. R., Al-Moosawi, L., Cummings, D. G., Harris, C., Kitidis,
882   V., Rees, A., Martinez-Vicente, V., and E. M. S. Woodward (2010). A broad
883   spatio-temporal view of the Western English Channel observatory. *J. Plankton*
884   *Res.,* **32**, 585-601. doi: 10.1093/plankt/fbp128
885

886   Son, S., Yoo, S., and J.-H. Noh (2006). Spring phytoplankton bloom in the fronts of
887   the East China Sea. *Ocean Sci. J.*, **41**, 181-189. doi:10.1007/BF03022423
888

889   Weston, K., Fernand, L., Mills, D., Delahunty, R., and J. Brown (2005). Primary
890   production in the deep chlorophyll maximum of the central North Sea. *J*
891   *Plankton Res*, **27**, 909–922.
892

893   Zhu, J., Hu, J., and Z. Liu (2013). On summer stratification and tidal mixing in the
894   Taiwan Strait, *Frontiers of Earth Science*, **7**, 141-150, doi:10.1007/s11707-013-
895   0355-1.

Figure Captions

897

898 Figure 1. Bottom depth (relative to sea surface) in the three S2P3-R domains: (a)
899 northwest European shelf; (b) western English Channel; (c) East China and Yellow
900 Seas.

901

902 Figure 2. Daily meteorological data: climatological for the northwest European shelf
903 (Sharples 2008), and for 2013 in the Western English Channel, and in the East China
904 and Yellow Seas: (a) air temperature; (b) wind speed; (c) cloud fraction; (d) relative
905 humidity.

906

907 Figure 3. For the northwest European shelf domain: (a) Hunter-Simpson parameter,
908 highlighting the contour delineating $\log_{10}(h/u^3) = 2.7$; (b) day 190 surface-bottom
909 temperature difference; (c) net surface heat flux; (d) annual net production. In (a), we
910 label fronts as in Fig. 8.1 of Simpson and Sharples (2012): the Islay front (A); the
911 Western Irish Sea front (B); the Cardigan Bay front (C); the St. Georges Channel
912 front (D); the Ushant and Western English Channel front (E). We additionally label
913 the Flamborough frontal system (F).

914

915 Figure 4. Sections through the Celtic Sea front around day 215 of 2003: (a) locations
916 of CTD stations (dots) and model grid-points (circles); (b), (c) observed and modelled
917 temperature (°C); (d), (e) observed and modeled dissolved inorganic nitrate (units
918 mmol m^{-3}); (f), (g) observed and modelled chl-a concentration (units mg chl-a m^{-3}).
919 The locations of observations in profile are indicated by dots in (b), (d) and (f).

920

921 Figure 5. Surface–bottom temperature differences (°C) in the Western English
922 Channel, on day 190 of 2002-13. Coloured circles indicate the coincident temperature
923 differences at L4 and E1, subject to data availability (E1 data are unavailable in 2004,
924 2006 and 2013).

925

926 Figure 6. Time series of surface-bottom temperature differences observed and (daily)
927 simulated at L4 and E1 (http://www.westernchannelobservatory.org.uk/data.php).

928

929   Figure 7. Sections through the developing tidal mixing front east of Lizard peninsula,
930   along 50.017°N, on days 100, 130, 160 and 190 of 2013: temperature (left column);
931   dissolved inorganic nitrate (mmol m^{-3}, middle column); chl-a (mg chl-a m^{-3}, right
932   column).

933

934   Figure 8. Time series of surface and bottom temperature (red and blue curves),
935   surface-bottom temperature difference, surface DIN and surface chl-a concentrations,
936   across the tidal mixing front east of the Lizard peninsula in 2013.

937

938   Figure 9. For the East China and Yellow Seas domain in 2013: (a) Hunter-Simpson
939   parameter, highlighting the contour delineating $\log_{10}(h/u^3) = 2.7$; (b) day 190 surface-
940   bottom temperature difference; (c) net surface heat flux; (d) annual net production.

941

942   Figure 10. Sections through the developing tidal mixing front of the East China Sea,
943   along 32°N, on days 100, 130, 160 and 190 of 2013: temperature (left column); DIN
944   (mmol m^{-3}, middle column); chl-a (mg chl-a m^{-3}, right column).

945

946   Figure 11. Surface-bottom temperature differences (°C) across the southern Celtic Sea
947   and western English Channel, in mid July of 2014, simulated with S2P3-R configured
948   in twelve 1° x 1° sub-domains, as indicated.

949   Table 1. Boundaries, resolution, tidal forcing, initial temperature and meteorological

950   forcing for each domain (POLCOMS = Proudman Oceanographic Laboratory Coastal

951   Ocean Modelling System; OTPS = OSU Tidal Prediction Software)

952

Domain	Boundaries	Resolution	Tidal Forcing	Initial temperature field	Meteorological forcing
northwest European shelf	14.917°W – 1.917°E 48.056°N – 61.944°N	0.167° (longitude) 0.111° (latitude) (~12 km)	M2, S2, N2 (POLCOMS)	10.1°C everywhere (default)	Daily climatology for the Celtic Sea (Sharples 2008)
Western English Channel	4 – 6°W 49.5 – 50.5°N	1' x 1' (~1 km)	M2, S2, N2 (POLCOMS interpolated)	10.1°C everywhere	Daily NCEP reanalysis data for grid square centred on 5°W, 50°N
East China and Yellow Seas	112 – 130°E 21 – 42°N	0.083° x 0.083° (~6 km)	M2, S2, N2, O1, K1 (OTPS)	After 1-year started from 15.1°C everywhere	Daily NCEP reanalysis data for grid square centred on 125°E, 32.5°N

953
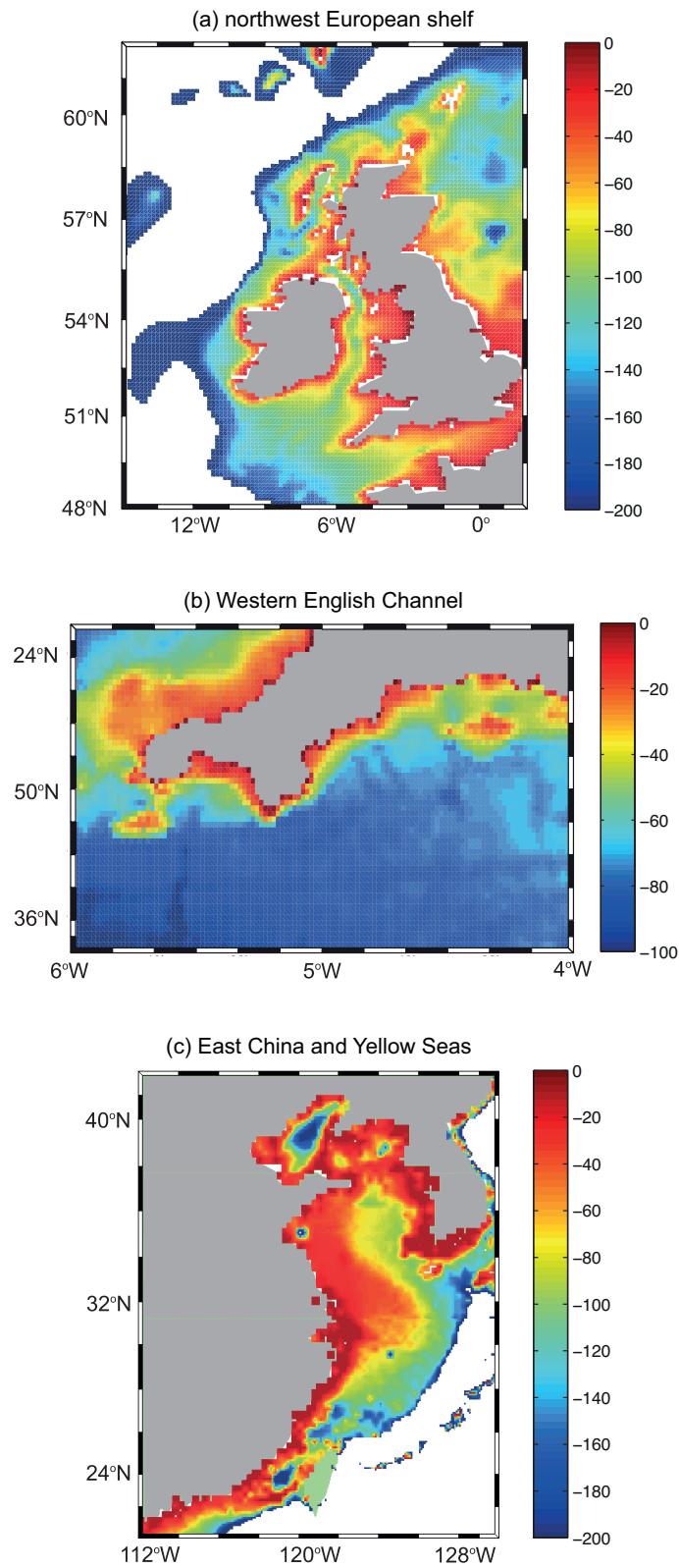
(a) northwest European shelf

(b) Western English Channel

(c) East China and Yellow Seas

Figure 1. Bottom depth (relative to sea surface) in the three S2P3-R domains: (a) northwest European shelf; (b) western English Channel; (c) East China and Yellow Seas.
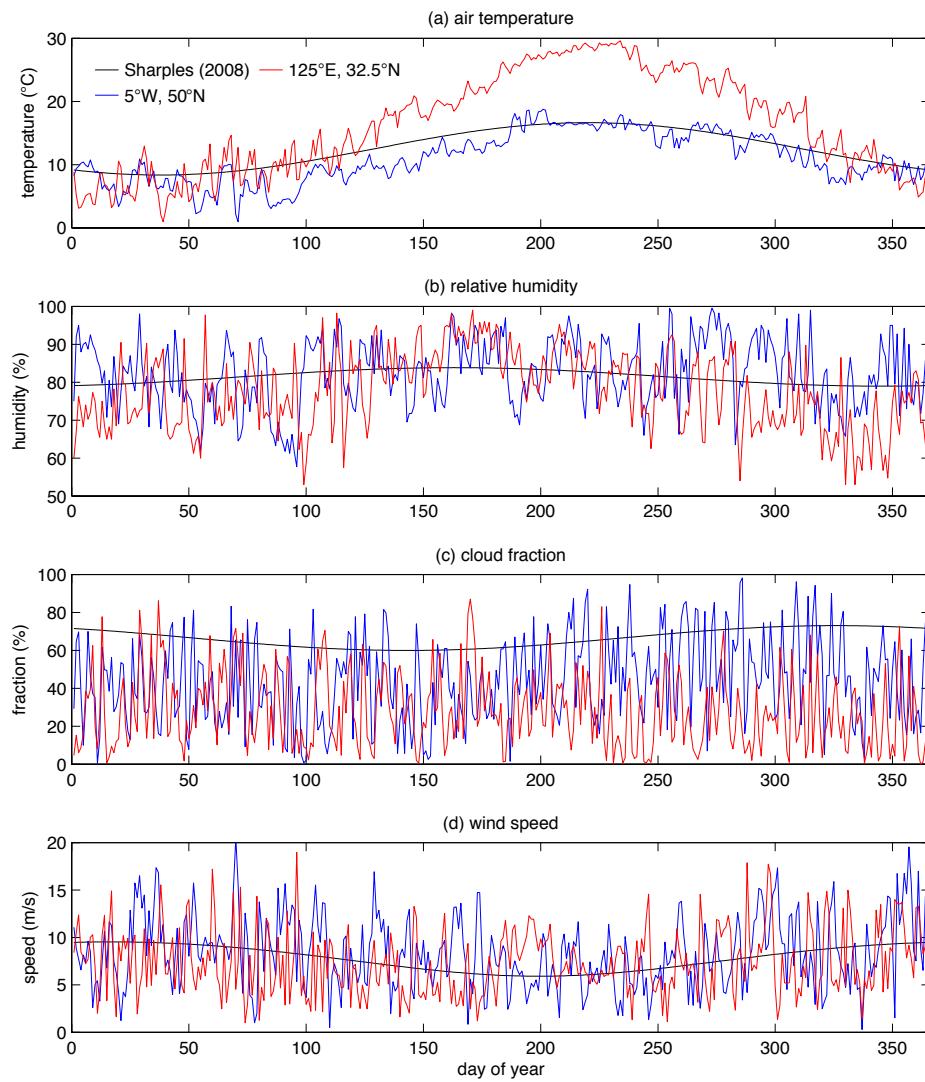
959

960   Figure 2. Daily meteorological data: climatological for the northwest European shelf

961   (Sharples 2008), and for 2013 in the Western English Channel, and in the East China

962   and Yellow Seas: (a) air temperature; (b) wind speed; (c) cloud fraction; (d) relative

963   humidity.

964

965

966

Figure 3. For the northwest European shelf domain: (a) Hunter-Simpson parameter, highlighting the contour delineating $\log_{10}(h/u^3) = 2.7$; (b) day 190 surface-bottom temperature difference; (c) net surface heat flux; (d) annual net production. In (a), we label fronts as in Fig. 8.1 of Simpson and Sharples (2012): the Islay front (A); the Western Irish Sea front (B); the Cardigan Bay front (C); the St. Georges Channel front (D); the Ushant and Western English Channel front (E). We additionally label the Flamborough frontal system (F).

35

(a) CTD stations (dots) and model gridpoints (circles)

(b) observed temperature

(c) model temperature

(d) observed nitrate

(e) model nitrate

(f) observed chlorophyll

(g) model chlorophyll

974

975   Figure 4. Sections through the Celtic Sea front around day 215 of 2003: (a) locations

976   of CTD stations (dots) and model grid-points (circles); (b), (c) observed and modelled

977   temperature (°C); (d), (e) observed and modeled dissolved inorganic nitrate (units

978   mmol m^{-3}); (f), (g) observed and modelled chl-a concentration (units mg chl-a m^{-3}).

979   The locations of observations in profile are indicated by dots in (b), (d) and (f).
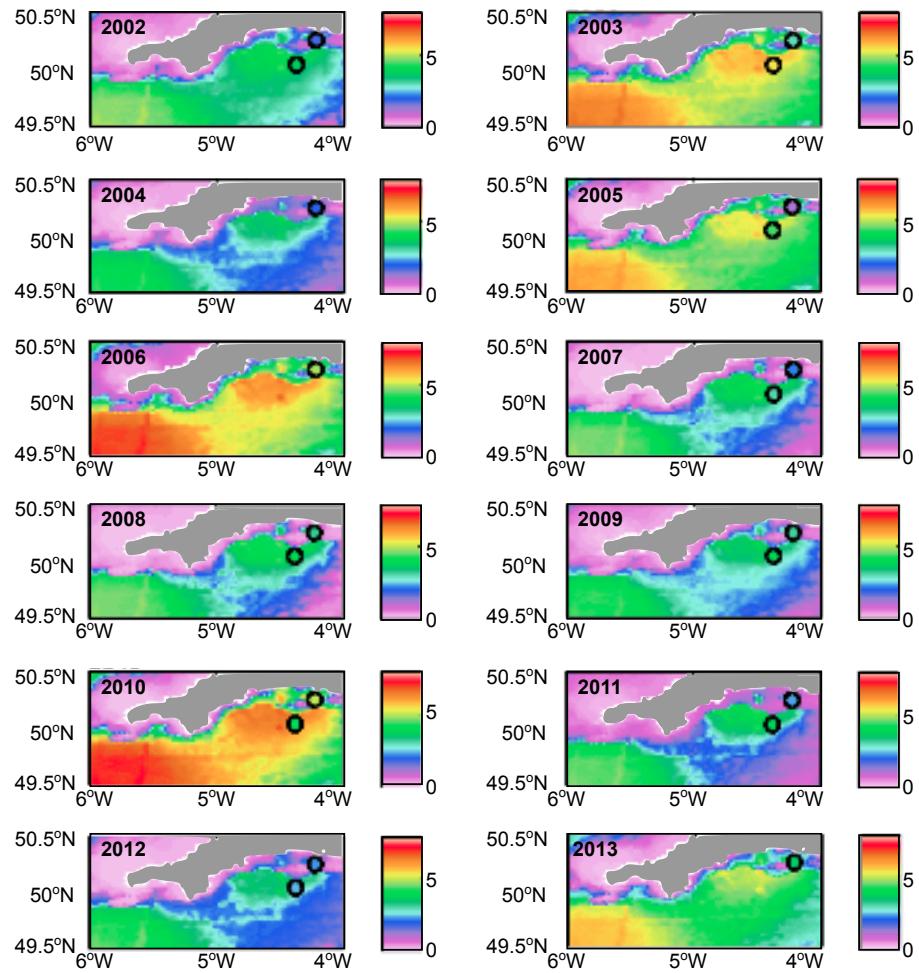
980

981

Figure 5. Surface–bottom temperature differences (°C) in the Western English Channel, on day 190 of 2002-13. Coloured circles indicate the coincident temperature differences at L4 and E1, subject to data availability (E1 data are unavailable in 2004, 2006 and 2013).
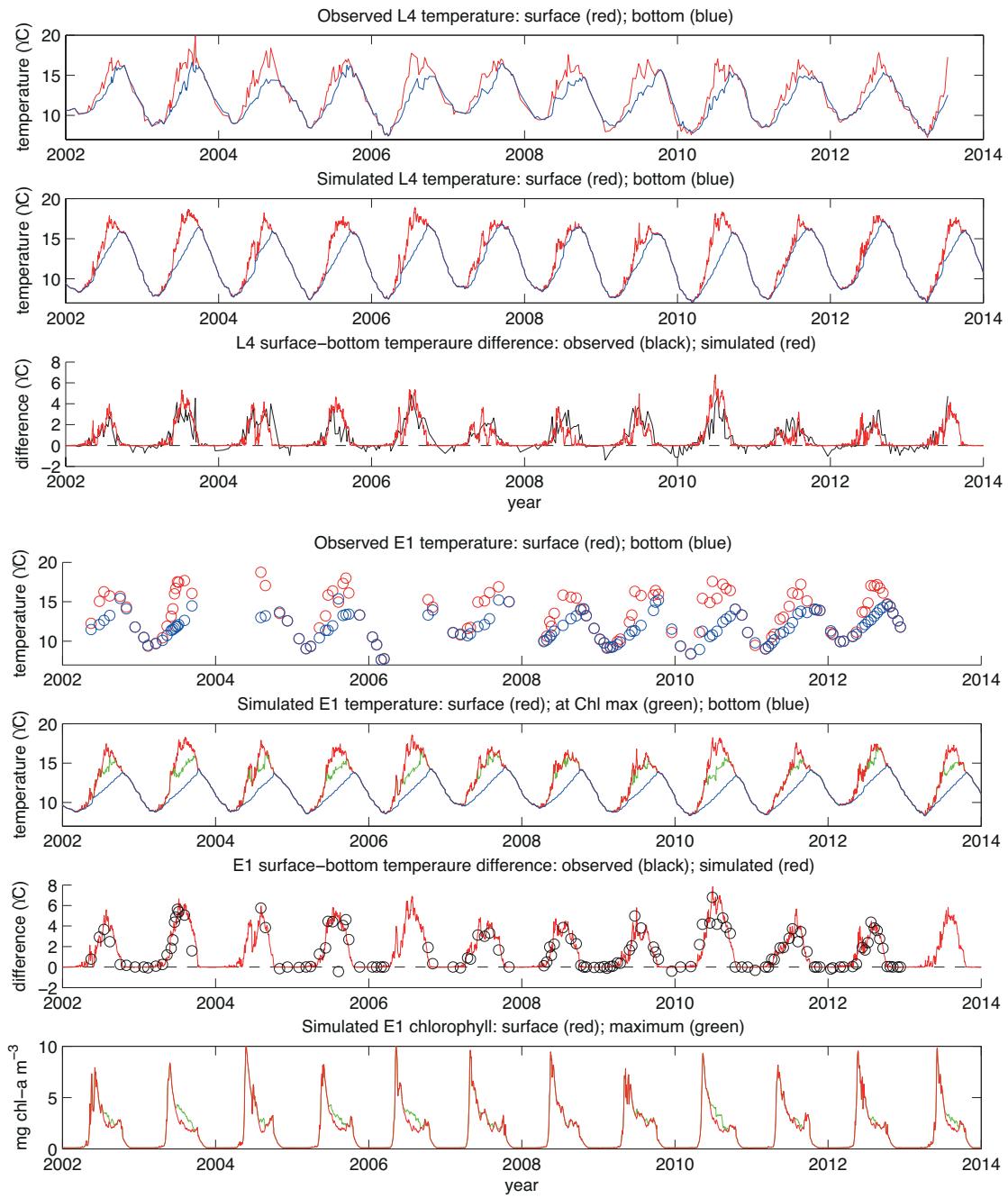
986

987

988 Figure 6. Time series of surface-bottom temperature differences observed and (daily)

989 simulated at L4 and E1 (http://www.westernchannelobservatory.org.uk/data.php).

38
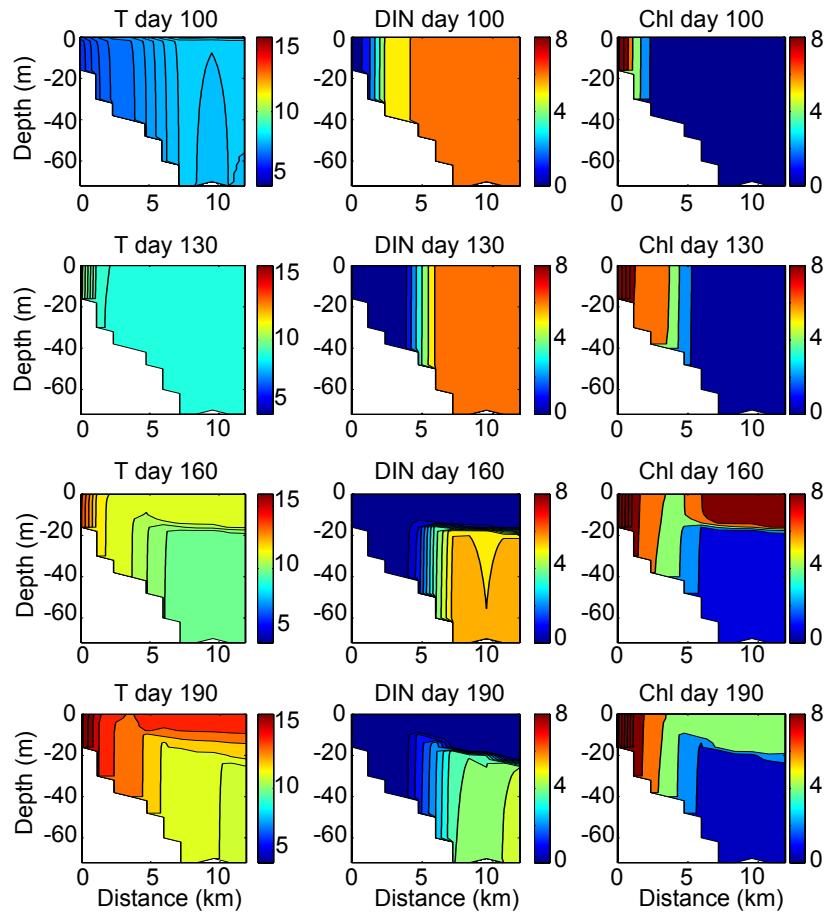
990

991

992　Figure 7. Sections through the developing tidal mixing front east of Lizard peninsula,

993　along 50.017°N, on days 100, 130, 160 and 190 of 2013: temperature (left column);

994　dissolved inorganic nitrate (mmol m^{-3}, middle column); chl-a (mg chl-a m^{-3}, right

995　column).
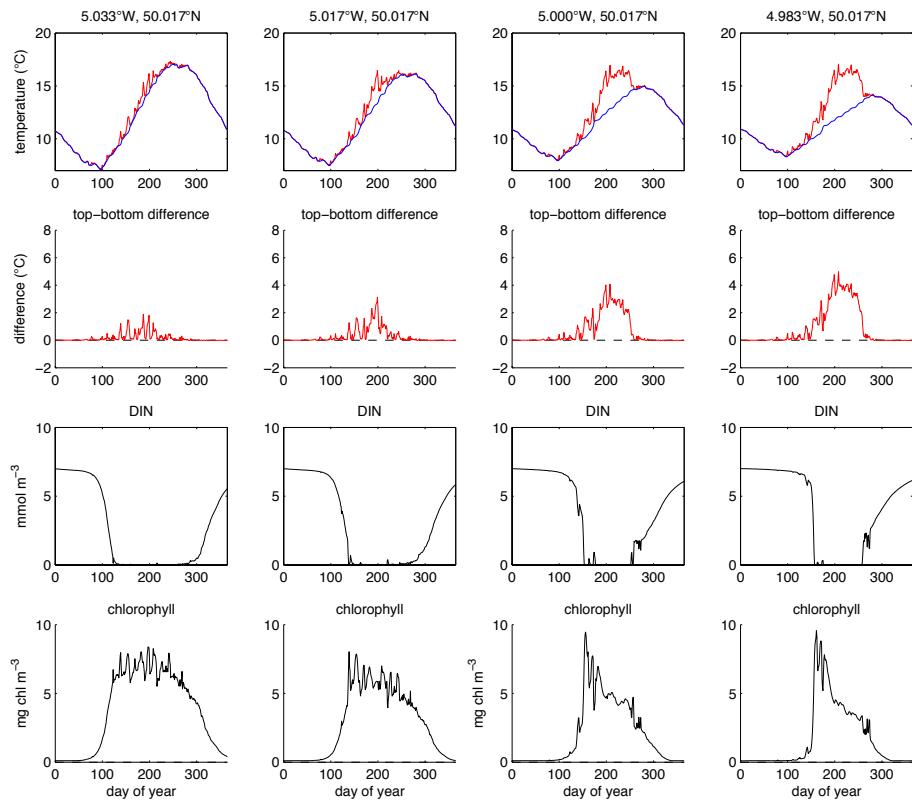
996

997 Figure 9. Time series of surface and bottom temperature (red and blue curves),

998 surface-bottom temperature difference, surface DIN and surface chl-a concentrations,

999 across the tidal mixing front east of the Lizard peninsula in 2013.
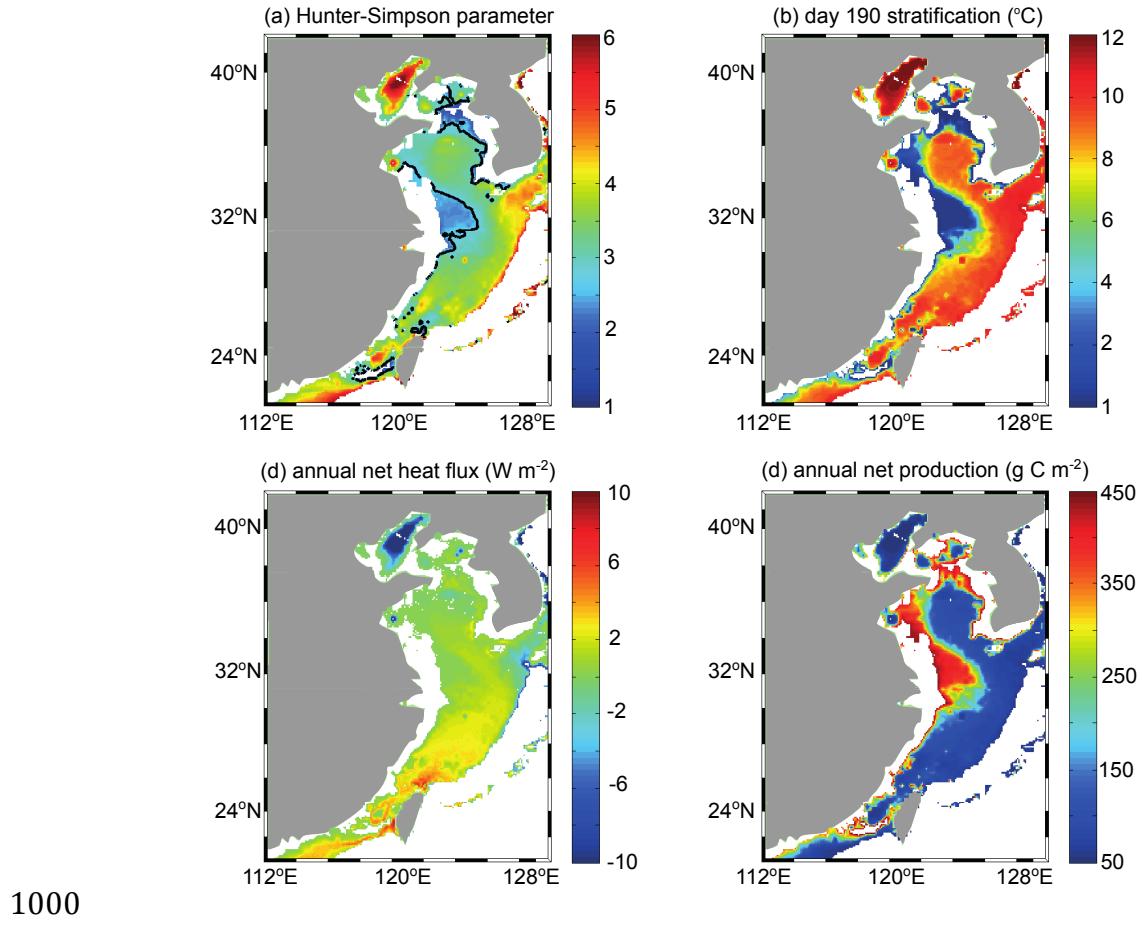
1000

1001

1002 Figure 9. For the East China and Yellow Seas domain in 2013: (a) Hunter-Simpson

1003 parameter, highlighting the contour delineating $\log_{10}(h/u^3) = 2.7$; (b) day 190 surface-

1004 bottom temperature difference; (c) net surface heat flux; (d) annual net production.

1005
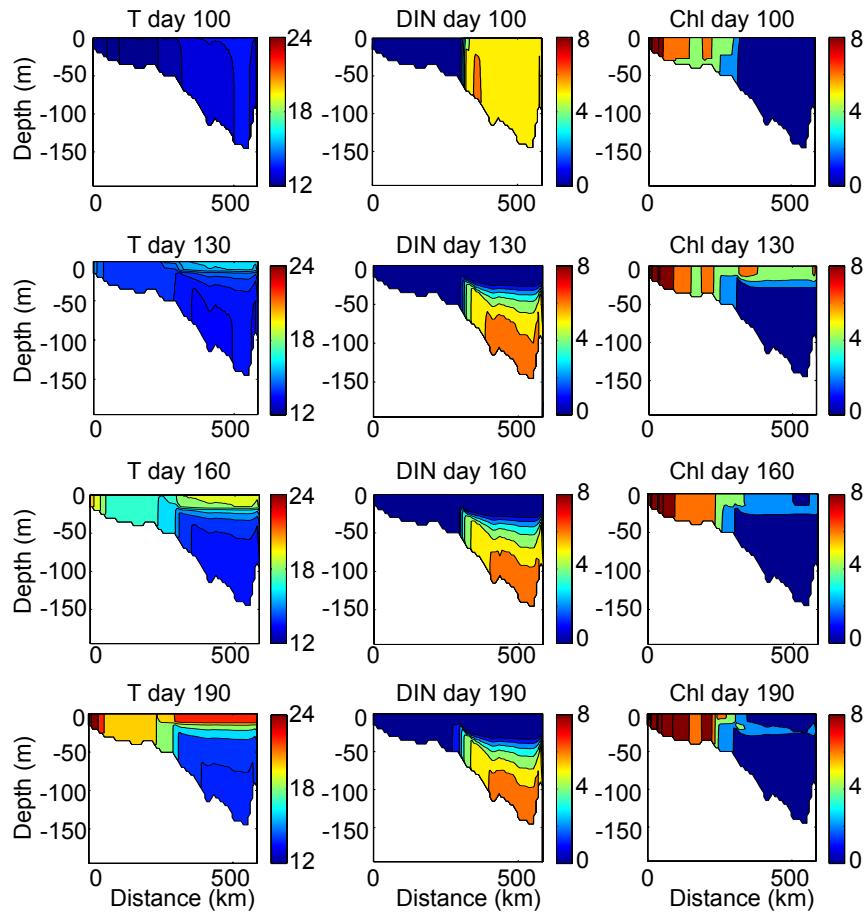
1006
1007
1008   Figure 10. Sections through the developing tidal mixing front of the East China Sea,
1009   along 32°N, on days 100, 130, 160 and 190 of 2013: temperature (left column); DIN
1010   (mmol m^{-3}, middle column); chl-a (mg chl-a m^{-3}, right column).
1011

1012
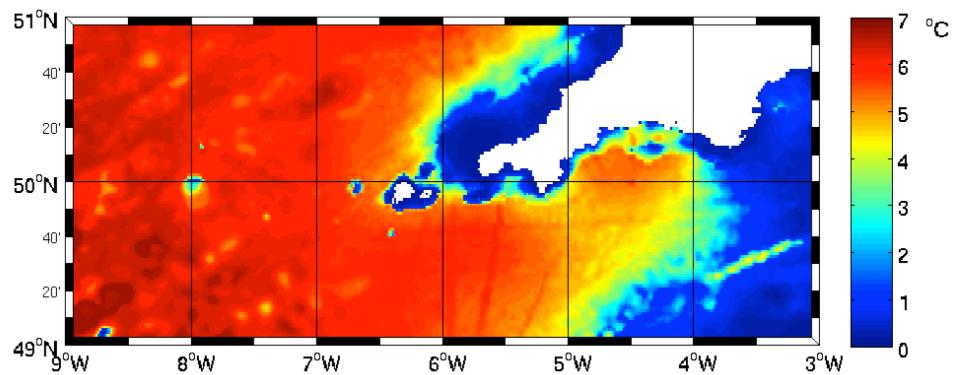
1013

1014   Figure 11. Surface-bottom temperature differences (°C) across the southern Celtic Sea
1015   and western English Channel, in mid July of 2014, simulated with S2P3-R configured
1016   in twelve 1° x 1° sub-domains, as indicated.